Spatial Estimation of Actual Evapotranspiration over Irrigated Turfgrass Using sUAS Thermal and Multispectral Imagery and TSEB Model

Karem Meza (karem.mezacapcha@gmail.com)
Utah State University
Alfonso F. Torres-Rua
Utah State University
Lawrence Hipps
Utah State University
William P. Kustas
United States Department of Agriculture
Rui Gao
Utah State University
Laura Christiansen
Utah State University
Kelly Kopp
Utah State University
Hector Nieto
Institute of Agricultural Sciences (CSIC)
Vicente Burchard-Levine
Spanish National Research Council (CSIC)
M Pilar Martín
Spanish National Research Council (CSIC)
Calvin Coopmans
Utah State University
Ian Gowing
Utah State University

Research Article

Keywords: Evapotranspiration, Eddy Covariance method, TSEB model, Unmanned Aircraft Systems, Leaf Area Index, Turfgrass

Posted Date: June 29th, 2023

DOI: https://doi.org/10.21203/rs.3.rs-3098168/v1

Additional Declarations: No competing interests reported.

Version of Record: A version of this preprint was published at Irrigation Science on December 6th, 2023. See the published version at https://doi.org/10.1007/s00271-023-00899-y.

Spatial Estimation of Actual Evapotranspiration over Irrigated Turfgrass Using sUAS Thermal and Multispectral Imagery and TSEB Model

[a]Karem Meza, [a]Alfonso F. Torres-Rua, [b]Lawrence Hipps,[c]William P. Kustas, [a]Rui Gao, [a]Laura Christiansen, [b]Kelly Kopp, [d]Hector Nieto, [e]Vicente Burchard-Levine, [e]M Pilar Martín, [f]Calvin Coopmans, [g]Ian Gowing

[a]Department of Civil and Environmental Engineering, Utah State University, Logan, UT 84322, USA

[b]Plants, Soils, and Climate Department, Utah State University, Logan, UT 84322, USA

[c]U.S. Department of Agriculture, Agricultural Research Service, Hydrology and Remote Sensing Laboratory, Beltsville, MD 20705, USA

[d]Institute of Agricultural Sciences (CSIC), Tec4AGRO Group, Serrano, 115b, 28006, Madrid, Spain

[e]Environmental Remote Sensing and Spectroscopy Laboratory (SpecLab), Spanish National Research Council (CSIC), 28037 Madrid, Spain

[f]Electrical and Computer Engineering Department, Utah State University, Logan, UT 84322, USA

[g]Utah Water Research Laboratory, Utah State University, Logan, UT 84322, USA

Abstract: Green urban areas are increasingly affected by water scarcity and climate change. The combination of warmer temperatures and increasing drought poses substantial challenges for water management of urban landscapes in the western U.S. A key component for water management, actual evapotranspiration (ETa) for landscape trees and turfgrass in arid regions is poorly documented as most rigorous evapotranspiration (ET) studies have focused on natural or agricultural areas. ET is a complex and non-linear process, and especially difficult to measure and estimate in urban landscapes due to the large spatial variability in land cover/land use and relatively small areas occupied by turfgrass in urban areas. Therefore, to understand water consumption processes in these landscapes, efforts using standard measurement techniques, such as the eddy covariance (EC) method as well as ET remote sensing-based modeling are necessary. While previous studies have evaluated the performance of the remote sensing-based two-source energy balance (TSEB) in natural and agricultural landscapes, the validation of this model in urban turfgrass remains unknown. In this study, EC flux measurements and hourly flux footprint models were used to validate the energy fluxes from the TSEB model in green urban areas at golf course near Roy, Utah, USA. High-spatial resolution multispectral and thermal imagery data at 5.4 cm were acquired from small Unmanned Aircraft Systems (sUAS) to model hourly ETa. A protocol to measure and estimate leaf area index (LAI) in turfgrass was developed using an empirical relationship between spectral vegetation indices (SVI) and observed LAI, which was used as an input variable within the TSEB model. Additionally, factors such as sUAS flight time, shadows, and thermal band calibration were assessed for the creation of

TSEB model inputs. The TSEB model was executed for five datasets collected in 2021 and 2022, and its performance was compared against EC measurements. For actual ET to be useful for irrigation scheduling, an extrapolation technique based on incident solar radiation was used to compute daily ETa from the hourly remotely-sensed UAS ET. A daily flux footprint and measured ETa were used to validate the daily extrapolation technique. Results showed that the average of corrected daily ETa values in summer ranged from about 4.6 mm to 5.9 mm in 2021 and 2022. The Near Infrared (NIR) and Red Edge-based SVI derived from sUAS imagery were strongly related to LAI in turfgrass, with the highest coefficient of determination (R^2) (0.76-0.84) and the lowest root mean square error (RMSE) (0.5-0.6). The TSEB's latent and sensible heat flux retrievals were accurate with an RMSE 50 W m^{-2} and 35 W m^{-2} respectively compared to EC closed energy balance. The expected RMSE of the upscaled TSEB daily ET estimates across the turfgrass is below 0.6 mm day^{-1}, thus yielding an error of 10% of the daily total. This study highlights the ability of the TSEB model using sUAS imagery to estimate the spatial variation of daily actual ET for an urban turfgrass surface, which is useful for landscape irrigation management under drought conditions.

Keywords: Evapotranspiration, Eddy Covariance method, TSEB model, Unmanned Aircraft Systems, Leaf Area Index, Turfgrass

1 Introduction

Urban green surfaces are a significant part of urban landscapes, especially in arid regions. Many of these are turfgrass-covered and include golf courses, parks, athletic fields, home lawns, and other urban green spaces. These landscapes provide benefits to society by contributing environmental and human health attributes (Maas et al. 2009; Braun et al. 2022a). However, urban turfgrass is negatively affected by increasing water scarcity caused by human demands and limited water supplies (Finley and Basu 2020; Braun et al. 2022b) and landscape water requirements can account for 40 - 75% of total municipal water use (Maupin et al. 2022). An 18-hole golf course, for example, has a median water use estimated at 11798 m^3 ha^{-1} per year or nearly 4 acre-feet which translates to approximately 1.3 million gallos per acre in the arid and warm Southwest United States (Gelernter et al. 2015). Evapotranspiration from lawns, trees, ornamental shrubs, and other plants is the primary water use in urban landscapes (Wynne and Devitt 2020). According to Braun et al. (2022a) the estimated cool-season turfgrass ET that is well-watered ranges from 5.35 to 7.79 mm day^{-1}. However, credible values for actual ET of cool-season turfgrass in arid regions are poorly documented as most studies use only crop coefficients for cool-season turfgrass and reference evapotranspiration (ETo) for the estimation of irrigation requirements. ETa is a complex and non-linear process that is difficult to measure and estimate in urban landscapes due to large spatial variability in land cover/land use (Saher et al. 2021), especially when drought conditions force managers to reduce or completely avoid irrigation in certain areas. Therefore, accurate spatial estimates of ETa in urban turfgrass are required for the management and planning of urban water resources (Litvak and Pataki 2016).

The most credible direct measurement of ETa is provided by the eddy covariance (EC) method (Nagler et al. 2005; Cuxart and Boone 2020). However, EC flux measurements may be inappropriate in some situations due to spatiotemporal limitations, system instrumentation, and data processing performed (Pastorello et al. 2020). Moreover, due to cost and logistical constraints, EC measurements cannot sample all land cover conditions. Therefore, to address the challenge of measuring ET and its spatial distribution, ET models are essential (Niu et al. 2020; García-Santos et al. 2022). Historically, simple models based on the Penman-Monteith equations failed to adequately consider soil-plant-atmosphere interactions, and physiological responses to environmental conditions above the canopy, as well as coupling between the surface and atmospheric conditions when the crop is not at optimal or expected conditions. On the other hand, surface energy balance (SEB) models have been developed in the past several decades to estimate spatial ET. One model that has been implemented and validated over multiple vegetation surfaces is the two-source energy balance (TSEB) model, which partitions the energy fluxes between canopy and soil/substrate by parameterization based on biophysical processes (Norman et al. 1995). Previous research has demonstrated the reliability of the TSEB model using sUAS information for estimating instantaneous evapotranspiration for vineyards (Nieto et al. 2019; Gao et al. 2022, 2023; Aboutalebi et al. 2022) and tree-grass ecosystems (Burchard-Levine et al. 2021; Simpson et al. 2022). However, no comparative evaluation and validation of the TSEB model exist for high-resolution imagery at local scales in green urban spaces (Saher et al. 2021).

Advanced techniques in aerial remote sensing platforms such as small unmanned aircraft systems (sUAS) equipped with thermal and multispectral sensors collect data at higher spatial and temporal resolution than satellites and are better able to address spatial heterogeneity of a complex landscape (Burchard-Levine et al. 2021; Nassar et al. 2022). The sUAS has been widely used in agricultural applications (Hassler and Baysal-Gurel 2019; Katz et al. 2022; Tang et al. 2022; Kumar Yadav et al. 2023), but less effort has been directed toward for turfgrass research. Multispectral imagery has been applied to derive spectral vegetation indices (SVI) and for use in turfgrass research to detect water stress (Badzmierowski et al. 2019), to evaluate the response to deficit irrigation (Marín et al. 2020), to estimate green cover percentage (Wilber et al. 2022; Wang et al. 2022), and to evaluate turfgrass quality (Zhang et al. 2019). Thermal imagery has been applied to estimate land surface temperature to detect early drought stress in turfgrass (Hong et al. 2019). In addition, sUAS thermal information and an ET model (i.e. 3T) have been used to estimate urban ET (Feng et al. 2022; Qin et al. 2022) but they did not validate the ET estimates with micrometeorological methods such as EC. The sUAS provides significant potential for monitoring and scheduling turfgrass irrigation (Mauri et al. 2022; Carlson et al. 2022), being necessary for a reliable, accurate estimation of ET.

The leaf area index (LAI) is a key biophysical input to the TSEB model for flux partitioning (Kustas et al. 2019; Burchard-Levine et al. 2020; Gao et al. 2022; Feng et al. 2023); and urban green surfaces are mostly covered by trees and turfgrass. Methods for ground-based LAI can be classified as direct or indirect. Direct methods are considered to be the most accurate but are time-consuming and labor-intensive. However, a direct method is needed for the validation of indirect methods (Weiss et al. 2004; Yan et al. 2019). The direct method consists of manually and destructively sampling leaves and measuring their areas with scanning techniques using instruments such as the LI-3000C Portable Leaf Area Meter (LI-COR, Lincoln, NE, USA), LI-3100C Area Meter (LI-COR, Lincoln, NE, USA), CI-202 Portable Laser Leaf Area Meter (CID Bio-Science, Camas, WA, USA). Indirect methods are generally faster and allow for a larger spatial sample to be obtained. One indirect method is the optical approach (LAI-2200C (LI-COR, Lincoln, NE, USA)) which is based on measuring the angular distribution of light transmission through canopies (Weiss et al. 2004; Yan et al. 2019). On the other hand, for urban turfgrass, there is a lack of instrumentation to measure and model ground-based LAI because of the short leaf length and narrow blade width. For example, in Kentucky bluegrass, the leaf heights range from 2.54 – 5.08 cm, and blade width ranges from 2-4 mm and the traditional methodology noted above is not applicable. Hence, there is a need for a protocol for estimating LAI of urban turfgrass for use as an input for the SEB model. Studies have developed a model to predict LAI in maize, peanut, wheat, and vineyards, where empirical methods were used to establish a statistical relationship between ground-based LAI and SVI (Zhu et al. 2018; Qi et al. 2020; Sarkar et al. 2021; Gao et al. 2022; Verma et al. 2022; Du et al. 2022; Wu et al. 2022), but no one has demonstrated the potential of UAS and SVI to predict and generate a LAI model for urban turfgrass. In contrast, a methodology has been developed to estimate LAI for individual trees using non-destructive optical instruments (Burchard-Levine et al. 2020). The LAI of individual trees is most often studied for isolated trees in urban settings, and is defined as the ratio of the total leaf area and crown projection area (Parker 2020).

Currently, quantifying water use from turfgrass under both watered and water-stressed periods requires two components. The first component is the best possible measurement of ETa. The second component is the validation of remote sensing-based model estimates of ET. Because of high spatial resolution UAS-based thermal and multispectral imagery, TSEB can be employed to model ET over green urban environments. To accomplish this, the main goal of this study was to evaluate the performance of the TSEB model employing UAS information for the estimation of ETa over irrigated turfgrass and then validate these estimates with EC measurements at a golf course near Roy, Utah, USA.

More specifically, the following questions were addressed:

(a) What are the daily ETa values for irrigated turfgrass over the summer irrigation season?

(b) How can LAI be quantified across a composite landscape of turfgrass and isolated trees?

(c) What is the accuracy of hourly and daily TSEB estimates of ET compared to EC measurements?

2 Materials and Methods

2.1 Study Area

The study was conducted at the Eagle Lake Golf Course in Roy, Utah, USA (41.15584 °N,112.050044 °W). The golf course consists of a driving range surrounded by fairways, greens, and sand traps, with low-density deciduous trees and various coniferous species. Buildings, a large parking lot, a miniature-golf course, and a municipal pool line the northern edge of the golf course (Fig.1). The driving range is planted with a mixture of Kentucky bluegrass (*Poa pratensis L.*) and perennial ryegrass (*Lolium perenne L.*) and is kept at a height of approximately 0.04 m. Figure 1a provides an aerial view of the golf course and the surrounding area, along with a marker indicating where the EC tower was located. The golf course was automatically irrigated, usually between the hours of 0000 and 0600 Mountain Standard Time (MST), but sometimes during the day also as determined by the superintendent using the ETo value calculated by the onsite weather station multiplied by a crop coefficient.

Fig 1. a) Map of Eagle Lake Golf Course and surrounding area, with the eddy covariance flux tower marked with a red circle, b) eddy covariance flux tower, and c) surface energy balance system.

2.2 Methodology

In this study, ET was modeled using the TSEB model with the Priestley Taylor (TSEB – PT) optim for the vegetation composited; and validated using EC measurements for a golf course in Roy, Utah, USA. A protocol to estimate destructive LAI in urban turfgrass areas was developed and ground LAI measurements were used to evaluate the empirical estimation of LAI using SVIs from high-resolution multispectral imagery. A schematic diagram illustrating the flow of data collection and processing, creation of inputs for the TSEB-PT model, and modeling and validation of the TSEB-PT model is shown in Fig. 2.

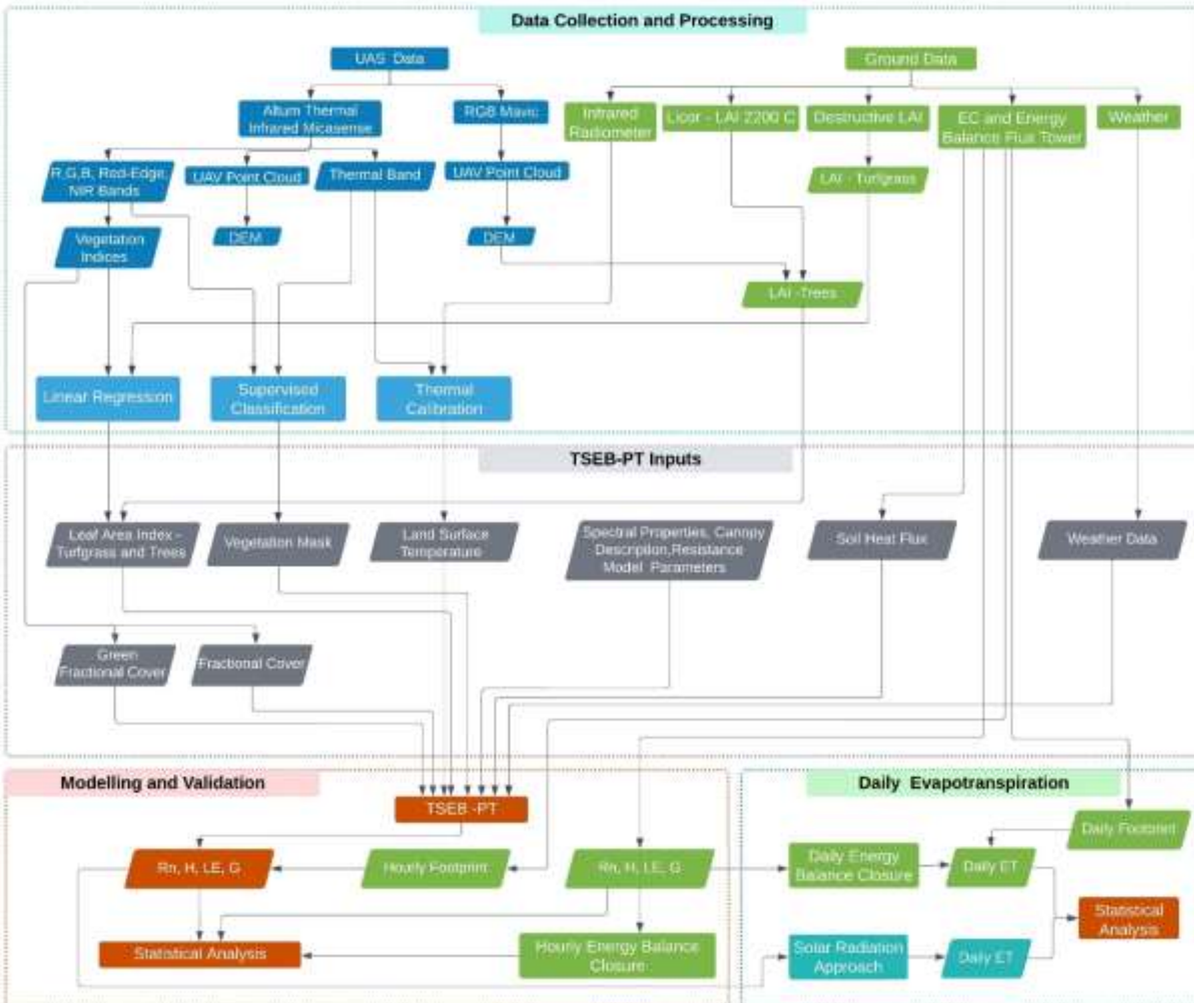

Fig 2. Flowchart illustrating the process of the study for assessing factors that affect the estimation of evapotranspiration (ET) in open green urban areas using high-resolution images captured by sUAS.

2.2.1 Data

- **Eddy-covariance and weather measurements**

The EC and energy flux tower was installed to collect flux measurements from July to October 2021 and April to October 2022, with prevailing winds at the site from the south-southwest during the growing season. Latent heat and sensible heat flux were measured at 2.6 m and 2.0 m above the ground in 2021 and 2022 respectively with an open-path infrared gas analyzer (LI-7500A, LI-COR Biosciences, Lincoln, NE, USA) and sonic anemometer (CSAT-3, Campbell Scientific, Logan, UT, USA). The CSAT-3 orientation was 214°. Sensor measurements were taken at a sampling rate of 20 Hz; and were stored in a high-performance CR 3000 datalogger (Campbell Scientific, Logan, UT, USA). Soil heat flux was determined using two soil heat flux plates (HFT-3.1; REBS, Seattle, WA, USA) at a depth of 0.06 m, four soil temperature sensors (Campbell Scientific, Logan, UT, USA) at depths from 0.015 to 0.06 m, and two soil moisture sensors (TDR -310H, Acclima, Inc., Meridian, ID) at depths of 0.04 and 0.1 m. Net radiation was measured using a four-component radiometer (SN-500-SS, Apogee Instruments, Logan, UT, USA) mounted 1.2 m above the surface in close proximity to the EC tower. Soil heat flux and net radiation measurements were averaged over 15 min periods and stored in a CR1000 datalogger (Campbell Scientific, Logan, UT, USA). Meteorological sensors were also placed at the EC tower. Air temperature, air humidity, wind speed, precipitation, and incoming solar radiation were measured and stored every 15 min to the CR1000 datalogger, which is part of the Utah State Climate Center network of weather stations (https://climate.usu.edu).

- **Collection, processing, and calibration of remote sensing imagery**

A rotary wing UAS DJI Matrice 600 Pro (DJI Technology Inc., Shenzhen, China) carrying an Altum camera (AgEagle Sensor Systems, Wichita, KS, USA) was used to collect imagery data. The camera has five high-resolution multispectral bands (blue, green, red, red edge, and near infrared) and an integrated long-wave thermal infrared (TIR) sensor (based on the FLIR Lepton) which was aligned with the multispectral sensors. Five flights were arranged via the AggieAir sUAS platform (https://uwrl.usu.edu/aggie air/) to acquire spectral and thermal information considering weather conditions and the Federal Aviation Administration (FAA) regulations for urban study locations. In Table 1, overpass time (MDT), sUAS altitude, multispectral and thermal pixel resolution, and weather conditions are listed for the overpass dates.

Table 1. Dates, times, flight height, spatial resolution, and weather to capture images with UAS

Date	Time (MDT)		UAS Elevation (m) AGL	UAS Spatial resolution (cm)	Weather
	Launch	Landing			
3-Sep-21	13:18 p.m	13:40 p.m	120	5.4	Sunny
21-Oct-21	12:59 p.m	13:21 p.m	120	5.4	Sunny
18-May-22	13:09 p.m	13:31 p.m	120	5.4	Sunny
20-Jul-22	14:15 p.m	14:40 p.m	120	5.4	Sunny
19-Sep-22	13:01 p.m	13:32 p.m	46	2.0	Sunny

For calibration of multispectral bands, images of the Altum calibration panel were taken before and after each flight from a height of approximately 0.5 m, with the panel clear of shadows. For each flight, an atmospheric correction of thermal data was computed to account for the effects of local weather and flight height conditions (Torres-Rua 2017). For calibration of the thermal band, an image of the blackbody temperature sensor (Fig. 3b) was taken and three infrared radiometers (Apogee Instruments, inc, Logan, UT, USA) were mounted on a tripod approximately 2 m above the ground and aimed at the center of a 3×3 m^2 reflectance panel (Fig. 3a). Nine AeroPoint ground control points (GCP) (Propeller Aero, Sydney, NSW, Australia) were placed for georeferencing each flight. Altum images were processed in Agisoft Metashape Professional v1.4.5 (Agisoft LLC, St. Petersburg, Russia) to create the point cloud data, digital elevation model, and orthomosaic.

Fig 3. a) Reflectance panels and three infrared radiometers for thermal band calibration and b) Altum camera calibration using reflectance panel and blackbody temperature sensor before the flight.

- **Leaf area index in turfgrass and trees**

A protocol was developed to estimate LAI in turfgrass. The LAI for Kentucky bluegrass was measured using a destructive sampling method. Turfgrass samples were collected on four dates (October 21, 2021, May 18, July 20, and September 19, 2022). For each date, green leaf samples were cut incorporating the low, medium, and high turfgrass qualities (color, uniformity, leaf texture, and density), which allowed a wide range of LAI value samples (Fig. 15 in Appendix). An AeroPoint GCP (Propeller Aero, Sydney, NSW, Australia) was placed to get reference coordinates for the samples across the golf course. Four samples per area of 3 × 3 m^2 were collected around the AeroPoint GCP, and a total of 216 green leaf samples were collected. To get consistent samples, a circular turfgrass sampler with an area 78.54 cm^2 was used to collect the green leaf samples (Fig. 16 in Appendix). The green leaf samples were cut from the plant and collected in labeled plastic bags which were placed in a cooled container until samples were processed in the laboratory. The green leaves were scanned at 300 dpi in an Epson Perfection V39 color scanner (Epson American Inc., Long Beach, CA, USA). Scan area was defined as 8.5 × 11.7 in^2. Leaf area was calculated from the scanned images using the unsupervised classification algorithm K-means, which is reliable for estimating the green cover in turfgrass plots (Wang et al., 2022). The mean value of each 3 × 3 m^2 area was calculated, which was then used as mean LAI. The LAI in turfgrass protocol and the python script developed to estimate the leaf area is available in the Hydroshare repository (Meza et al. 2023).

The LAI for individual trees was measured with an LAI 2200 C plant canopy analyzer (Li-Cor Biosciences, Lincoln, NE, USA). Data collection and processing of raw data were completed according to the protocol developed and tested by the Environmental Remote Sensing and Spectroscopy Laboratory (Speclab (Burchard-Levine et al. 2021). Tree LAI measurements were collected from 10:00 am to 12:00 pm under clear sky conditions. The below-tree measurements were performed at two positions within each isolated tree using the 90° cap as LAI measurements in isolated trees should avoid the solar azimuth angle and its opposite angle when data is acquired under direct illumination conditions. To avoid the solar azimuth angle and its opposite angle, a compass was fixed on the optical sensor wand for reading the azimuth angles for each measurement point. In addition, a wooden ruler measuring 95 cm was attached to the plant canopy analyzer using a zip tie for standardizing the sensor height below the trees. The above measurements were taken two times per position at 6 m horizontally from the isolated tree using the 90° cap. A 3D reconstruction using an RGB camera on an UAS was conducted to delineate the tree crown and to obtain tree height. Photos from the RGB camera were used to generate a canopy digital surface model. We acquired an oblique image set 30º from the nadir. The overlap rate of the sUAS flight course heading and side direction was 80% and 75%, respectively, at a flying height of 60 m. Considering the particularity of the view of oblique photography, we used an orthogonal flight to obtain oblique photos, which was implemented in two phases (N–S and E–W). The images were processed in Agisoft Metashape Professional v1.4.5. Once the raw data of LAI, azimuth angles of the tree reading, zenith angles of a solar position, and coordinates of the tree profile were collected, the dripline LAI for the isolated trees were determined using FV 2200 software (Li-Cor Biosciences, Lincoln, NE, USA)

2.2.2 Daily actual evapotranspiration for irrigated turfgrass over the summer irrigation season

- **Eddy-covariance data processing and quality control**

High-frequency raw data from 2021 and 2022 were processed with a 1 hr. averaging interval using Fortran program developed by our laboratory. Before calculating the fluxes, low-quality raw data were screened out based on automatic gain control (AGC) values from the infrared gas analyzer and diagnostic values from the sonic anemometer (Pahari et al. 2018). A python script was accessed via a Jupyter Notebook for removing raw data with values of AGC above 70. Abnormal AGC values were due to precipitation times and accumulation of carbonates caused by secondary water used for irrigation. Elimination of spikes based on standard deviation (SD) of slidiry windows was applied to raw data water vapor density, sonic temperature, and wind speed (U_X, U_y, U_z). Data five times greater than the SD was removed as spikes using the Fortran program. The latent and sensible heat fluxes were calculated with correcting including wind coordinate rotation, Webb-Pearman-Leuning corrections for density effects (Webb et al. 1980), and the frequency response and path length, of the sensors (Massman and Lee 2002). Gap-filling was performed using the ReddyProc R package (Wutzler et al. 2018).

- **Energy balance closure of eddy-covariance measurements**

The surface energy balance at a surface obeys the following simplified equation:

$$R_n - G - LE - H = 0 \qquad \text{Eq. 1}$$

Where R_n is the net radiation, G is ground heat flux, LE is latent heat flux, and H is sensible heat flux in Wm^{-2}. The hourly flux data of the four terms were filtered considering the values of R_n>50 Wm^{-2}. Where values are large enough to check the balance of Eq. 1. These fluxes were used to calculate the ratio of the sum of turbulent fluxes to the available energy. This ratio is called the energy balance closure (EBC) and allows us to assess the reliability or quality of measurements of turbulent fluxes.

$$EBC = \frac{H+LE}{R_n-G} \qquad \text{Eq. 2}$$

For EC measurements, typical closure ratios can range from 0.7 to 0.9, where higher closure ratios suggest more consistency of measurements.

Most of the energy balance closure studies reported more assessments at daily, rather than hourly, timesteps (Wilson et al. 2002; Foken 2008; Stoy et al. 2013). The Bowen-ratio (β) method was used for daytime fluxes, considering the values of $R_s > 0$ Wm^{-2}. When the closure is forced, the extra flux will be assigned to both the sensible and latent heat flux.

$$\beta = \frac{H}{LE} \qquad \text{Eq. 3}$$

$$LE = \frac{R_n - G}{\beta + 1} \qquad \text{Eq. 4}$$

- **Daily actual evapotranspiration**

The corrected daily ETa (ET_{D_C}) was calculated as the sum of daytime eddy covariance ET fluxes (LE_{DT_B}) corrected by EBR partitioned based on a daily mean β plus the sum of nighttime eddy covariance ET fluxes (LE_{NT}) at positive values.

$$ET_{D\_C} = \frac{1}{\rho_w} \times \frac{LE_{DT\_B} + LE_{NT}}{\lambda} \qquad \text{Eq. 5}$$

Where ρ_w (kg m^{-3}) is the density of water, and λ (MJkg^{-1}) is the latent heat of vaporization.

2.2.3 Spectral vegetation indices for LAI estimation in turfgrass

Six SVIs were selected based on their characteristics to study LAI. Different SVIs were computed, such as OSAVI, NDRE, NDVI, MSR, and Ln(RVI), which are known as a predictors of LAI (Qi et al. 2020; Sarkar et al. 2021; Verma et al. 2022; Du et al. 2022). Additionally, one SVI was generated by the Eureqa software (Gashaw et al., 2022), which uses symbolic regression to select the best model for the given dataset. Centered on the point where LAI was measured, regions of interest (ROIs) with a size of 3 × 3 m^2 were clipped from the digital image. The zonal statistics tool from ArcGIS PRO v3.0.2 (ESRI, Redlands, CA, USA) was used to extract the red, red-edge, and NIR information of turfgrass and compute the SVI from ROIs. Table 2 shows the selected SVIs and their equations.

Table 2. Spectral vegetation indices selected for estimation of LAI in turfgrass

Spectral Vegetation Index	Equation	References
Optimized Soil–Adjusted Vegetation Index (OSAVI)	$OSAVI = \frac{(1+0.16) \times (NIR - Red\ Edge)}{NIR + Red\ Edge}$	Rondeaux et al.,1996
Normalized Difference Red – Edge Index (NDRE)	$NDRE = \frac{NIR - Red\ Edge}{NIR + Red\ Edge}$	Gitelson et al.,1994
Normalized Difference Vegetation Index (NDVI)	$NDVI = \frac{NIR - Red}{NIR + Red}$	Rouse et al.,1974
Modified Red- Edge Simple Ratio Index (MSR)	$MSR = \frac{\frac{NIR}{Red\ Edge} - 1}{\sqrt{\frac{NIR}{Red\ Edge} + 1}}$	Chen et al.,1996
Ln - Ratio Vegetation Index	$Ln(SR) = Ln(\frac{NIR}{Red\ Edge})$	First used for this study

Eureqa Index	$EUR = \left(1.7 \times \frac{NIR}{Red\ Edge}\right) - 1.9$	First used for this study

The six SVIs were used as independent variables and LAI ground measurements as dependent variables. The linear regression method was applied to predict LAI in turfgrass, and the accuracy of the model was evaluated by the R^2 and RMSE (Eqs.6-7).

$$R^2 = 1 - \frac{\sum_{i=1}^{n}(M_i - E_i)^2}{\sum_{i=1}^{n}(M_i - \bar{M}_i)^2} \quad \text{Eq. 6}$$

$$RMSE = \sqrt{\frac{\sum_{i=1}^{n}(M_i - E_i)^2}{n}} \quad \text{Eq. 7}$$

Where n is the number of records, M_i is an observation, E_i is the estimated value, and $\bar{M}_i$ is the average observation.

2.2.4 Two source energy balance and its validation

- **Two source energy balance (TSEB) and Priestley Taylor (PT) model**

The TSEB model was developed by Norman et al. and Kustas and Norman (1995; 1999). TSEB estimates latent heat flux as the residual of the surface energy balance. Formulas and more details have been published in previous research (Xia et al. 2016; Cheng and Kustas 2019; Nieto et al. 2019; Simpson et al. 2021; Gao et al. 2022; Nassar et al. 2022) for agricultural and natural ecosystems. The TSEB - PT approach was used to model ET in an urban ecosystem (Fig.4), and an open-source python repository (https://github.com/hectornieto/pyTSEB (accessed on 2 September 2022)) was used to calculate energy fluxes. R_n is net radiation, H is sensible heat flux, LE is the latent heat flux and G is the soil heat flux. Subscripts "S" and "C" represent the soil and canopy components, respectively.

Table 3 contains the main list of inputs and data sources for trees and turfgrass cover. Land surface temperature (LST), LAI, fractional cover (f_c), and green ground cover (f_g) raster were aggregated to 3m resolution. The processing methods are explained in the following sections.

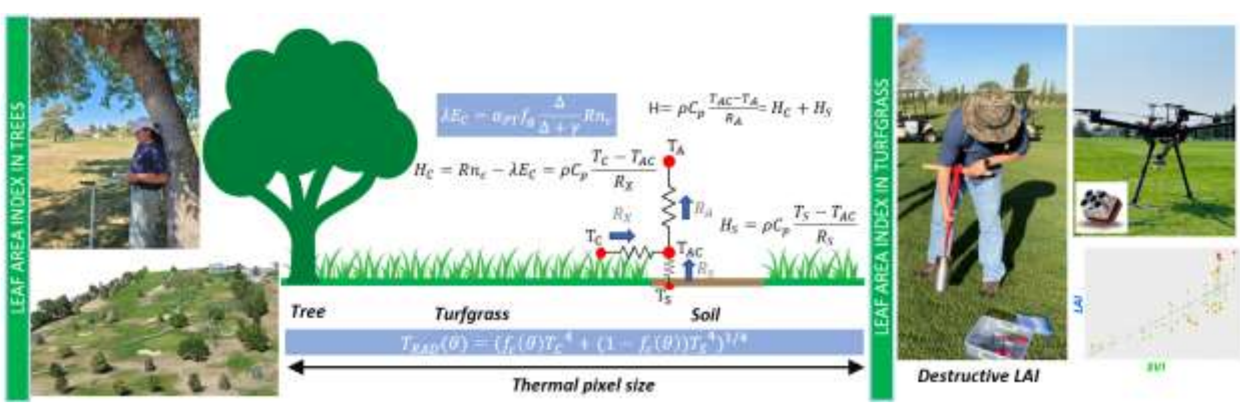

Fig 4. Schematic representation of the Two-Source Energy Balance (TSEB) Priestley Taylor approach.

Table 3. LST, biophysical, weather variables, and parameters for the TSEB-PT model.

Variable /parameter	Turfgrass	Trees
Radiometric composite temperature (K)	Land Surface Temperature (LST)	
Effective Leaf Area Index (m^{-2} m^{-2})	Empirical LAI model	LAI-220CC measurements
Fractional cover (0-1)	NDVI > 0.55, fractional cover (f_c) =1	
Green ground cover (0-1)	($NDVI-NDVI_{min}$/ $NDVI_{max}-NDVI_{min}$)	
Average canopy height (m)	0.0345	12
Weather	https://climate.usu.edu/	
Leaf angle distribution	1	1
Canopy wide-to-height ratio (m/m)	1	1
Resistance parameter b	0.012	0.034
Resistance parameter c (m s^{-1} $K^{-1/3}$)	0.0025	0.0025
Resistance parameter C' ($s^{1/2}$ m^{-1})	90	90
Effective leaf width (m)	0.01	0.05
Bare soil aerodynamic roughness length (m)	0.01	0.01
Priestley – Taylor parameter	1.26	1.26

- **Land surface temperature, Leaf area index, Fractional cover, Green ground cover, and Canopy height**

The key TSEB-PT model input data from sUAS information included maps of LST, LAI, f_c, and f_g. The LST map was created using the thermal band corrected with an environment-able blackbody instrument and infrared thermometer sensors (IRTs). The LST map contains radiometric surface temperature $T_{RAD}(\theta)$ pixel values that combine temperatures emitted by vegetation and the soil surface. Turfgrass canopy temperature (T_c) is important for understanding turfgrass physiological responses to the environment (Hong et al. 2019).

The TSEB-PT model requires vegetation biophysical properties such as LAI, f_c , f_g,and canopy height (Table 3). The LAI-turfgrass imagery was estimated using an empirical LAI-SVI relation. LAI-tree measurements were averaged, and an LAI-tree raster was created with the average LAI. This method for estimating LAI has been explained in section 2.2.1 above, LAI data collection.

The high spatial resolution of multispectral imagery (Table 1) allows separation of turfgrass and tree canopies from the impervious areas. Normalized difference vegetation index (NDVI) imagery was used to estimate vegetation cover (French et al. 2003; Simpson et al. 2021; Nassar et al. 2022) and pixels were classified into vegetation and vegetation categories by ArcGIS Pro image processing software. Fractional cover, f_c, was calculated with NDVI. Pixels with NDVI values greater than 0.55 were assigned f_c equal to 1. f_c is relevant for the partitioning of $T_{RAD}(\theta)$ into component soil, T_S, and canopy temperature, T_C. Green ground cover, f_g, was calculated following the approach of (Gutman and Ignatov 1998), which is based on minimum and maximum NDVI. f_g is the green fraction with active transpiration and photosynthesis; and is part of the Priestley Taylor formulation.

- **TSEB-PT model parameters**

The TSEB-PT model parameters such as leaf angle distribution, canopy wide-to-height ratio, resistance parameters, effective leaf width, bare soil aerodynamic roughness length, and Priestley – Taylor parameter are listed in Table 3.

The distribution and structure of foliage in the vegetative layer have a substantial influence on the dynamics of radiation interception and transmission through the canopy. Sparse vegetation is generally clumped and tends to intercept less radiation for the same LAI compared to vegetation randomly dispersed over the surface. TSEB model estimates the clumping index, which quantifies the spatial distribution of foliage to account for non-randomness in vegetated structures (Campbell and Norman 1998; Kustas and Norman 1999). Leaf angle distribution and canopy width-to-height ratio parameters were used to compute the clumping index.

The TSEB-PT model requires aerodynamic resistance (Ra, Rs, Rx) parameterizations (Fig.4) for the flux exchange above the canopy layer, within the canopy air space and at the soil/substrate surface. Resistance b and c coefficients were used to compute the resistance to heat flux in the boundary layer above the soil surface (Kustas and Norman 1999). Resistance parameter C' is derived from the weighting coefficient for leaf boundary layer resistance over the height of the canopy (McNaughton and Van Den Hurk 1995). Bare soil aerodynamic roughness length (z_0) and effective leaf width were inputs to compute the aerodynamic resistance Rx and Rs (Norman et al. 1995).

Priestley – Taylor parameter (α_{PT}) was used for the initial canopy transpiration estimate using the Priestley – Taylor formulation. The α_{PT} =1.26 is used as a first estimate for the model initialization (Agam et al. 2010)

- **Considerations for the creation of TSEB raster inputs**

Flight times

sUAS flights were conducted on days with appropriate weather conditions: clear skies, moderate wind (fly under 12 ms^{-1}), and atmospheric stability. The sUAS imagery was collected around solar noon (between 1:00 pm and 2:40 pm) for capturing the period of highest ET in turfgrass and trees and for minimizing tree canopy and building shadows. We also avoided times when activities (irrigation events, turfgrass mowing, tree crow thinning, and others) and tournaments were occurring at the golf course.

Spatial resolution

High spatial and temporal resolutions are critical for accurately estimating ET in heterogeneous urban landscapes with a combination of turfgrass and isolated trees in water-limited cities (Nouri et al. 2020; Feng et al. 2022). The 3 m pixel size of the TSEB raster inputs was small enough to discriminate turfgrass, trees, sidewalks, sand traps, and building signals. According to Burchard-Levine et al. (2021), the thermal sharpening of less than 5 m was able to discriminate grassland and trees, and they reported that TSEB accurately simulated hourly ET with Root Mean Square Deviation (RMSD) ~ $60Wm^{-2}$.

Thermal band calibration

Blackbody temperature and IRT sensors were used to correct the bias of the UAS thermal imagery. The first thermal correction was made using a blackbody temperature sensor and; the correction values varied from 0.9 to 2.6 °C. The second thermal correction using IRT sensors showed a strong positive relationship with R^2=0.98 and RMSE=3.5 °C (Fig.18 in Appendix). This result agreed with studies reported by Brewer et al. (2022) on the atmospheric correction of Micasense Altum thermal imagery using IRTs. ET estimations using SEB models potentially have systematic errors due to inherent calibration bias of land surface temperature data in urban regions (Liu Wenjuan et al. 2010). By increasing the accuracy of sUAS thermal imagery, agricultural and urban studies that utilize this information for estimating ET will benefit greatly and resulting in better water management decisions.

Land cover classification based on UAS data

Turfgrass and tree masks based on sUAS images were fundamental for running the TSEB model because turfgrass and trees have different inputs for LAI, LST, and parameters for estimating ET. However, the golf course also had high spatial variability, containing classes such as vegetation, sidewalks, sand traps, buildings, and other non-vegetation objects. The UAS images, segmentation, and supervised classification using the Random Trees model from ArcGIS Pro were applied to classify the golf course into five categories: turfgrass, trees, non-turfgrass, sand, and shadows. This classification method required image segmentation which was used to train the classifier (Park et al., 2022). Image segmentation used NIR, red, and blue bands from UAS data was identified as the effective bands for classifying land cover types in an urban environment. Segmented raster, thermal band, and 860 training sample polygons were inputs for training the classifier. The classifier definition file and the thermal band were used for the classification of the raster. Confusion matrix, kappa coefficient, and overall accuracy were used for accuracy assessment.

Figure 5a shows the classification map, the percentage for each class was: turfgrass (84%), trees (3%), non–turfgrass (11%), sand (1%), and shadows (1%). NIR, red, blue, and LST were effective inputs for the land cover map classification; turfgrass and trees were distinguished from non-turfgrass. Most previous studies have used multispectral and LST images acquired from UAS for urban area classification (Hartling et al. 2021; Park et al. 2022; Lee et al. 2023). The classification accuracy results indicate that Random Trees accuracy was 95% and Kappa was 0.94. This showcases the benefit of UAS data in complex urban green areas to separate non-turfgrass features such as trees, sand traps, shadows, and impervious areas.

Shadows

Shadow classification over high-resolution UAS imagery is important to avoid a negative impact on the supervised classification results and estimation of ET in almonds, vineyards, and peaches (Park et al. 2021; Mokhtari et al. 2021; Lu et al. 2022) due to shadows in remote-sensing data degrading the quality of spectral (Milas et al. 2017) and thermal information (Aboutalebi et al. 2019a; Mokhtari et al. 2021). As was explained in the section above, supervised classification was computed for shadows (Fig. 5 a), which had better performance than unsupervised classification or clustering, index-based, and physical-based methods applied in vineyards (Aboutalebi et al. 2019a). Figure 5 b, c, d, and e, illustrate the false color image in which black pixels show shadows for the different flight dates and times. Shadow magnitude and direction changed over time. Therefore, a supervised classification is recommended for each flight.

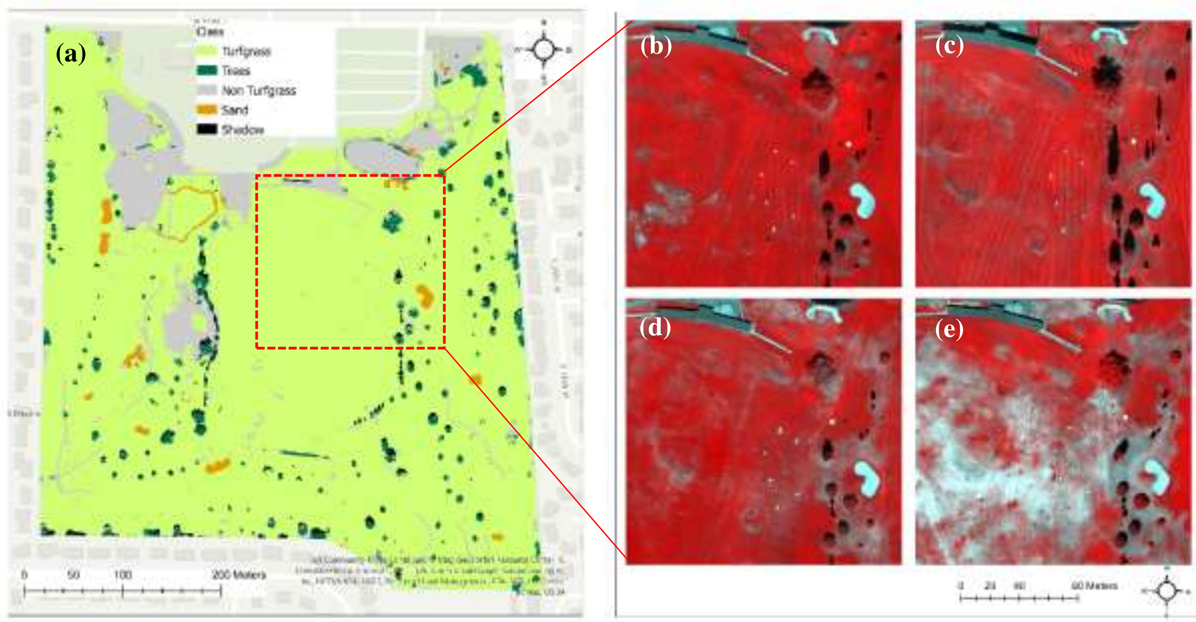

Fig 5. a) Supervised classification map of the Eagle Lake Golf Course on May 18, 2022, b) UAS false color on 3 September 2021 c)21 October 2021 d) 18 May 2022, and e) 20 July 2022

- **TSEB-PT model and Eddy-Covariance Tower Energy Fluxes**

Comparisons of remotely sensed ET versus the EC flux measurements were made using a flux footprint for a sampling of pixels in the source area of the flux tower (Gao et al. 2021; Volk et al. 2023) The flux footprint can be defined as the source (or sink) area of flux observation from EC measurements, the location and extent of which depend primarily on measurements of height, wind direction, wind speed, atmospheric stability, and roughness length (Kljun et al. 2015). The hourly flux footprints were computed with the Kljun et al. (2015) 2-dimensional model using a Python version available at https://footprint.kljun.net/. The footprint fetch was defined by the maximum distance from the EC tower location to the 90% footprint climatology contour. The EC daytime hour data were selected for hourly flux footprint based on the UAS flight time. The spatial resolution was 3 m, which is the same as the TSEB - ET raster.

The estimated energy fluxes Rn, H, LE, and G (W m^{-2}) by TSEB-PT were extracted using the hourly flux footprint model. These modeled energy fluxes were compared to the observed (non-closed and closed energy balance) fluxes by the EC tower. To assess the TSEB-PT model's accuracy and compare the model results with the non-closed and closed energy balance, we use the R^2 and RMSE, mean absolute error (MAE), and relative root mean square error (RRMSE) (Eqs.6-9).

$$MAE = \frac{\sum_{i=1}^{n} |M_i - E_i|}{n} \qquad \text{Eq. 8}$$

$$RRMSE = \frac{RMSE}{\overline{M_i}} \times 100 \quad \text{Eq. 9}$$

- **Daily evapotranspiration from scaling model and observed daily actual evapotranspiration**

A scalar extrapolation technique based on incident solar radiation was used to compute daily ETa from the hourly remote-sensed UAS-ET. This technique was developed by Jackson et al. (1983), who proposed that ET is highly correlated to incoming solar radiation. According to Colaizzi et al. (2006), the best time for extrapolating hourly ET to a daily scale is within 1 or 2 hours of solar noon. Other studies have reported that the incoming solar radiation extrapolation technique worked relatively well for crops and describing daily and hourly evapotranspiration (Wandera et al. 2017; Nassar et al. 2021).

$$ET_d = \left(\frac{LE}{R_s}\right)\left(\frac{c}{\rho_w \lambda}\right) R_{s24} \quad \text{Eq. 10}$$

Where ET_d is daily (24 h) total ET (mm d^{-1}), LE is latent heat flux (W m^{-2}), R_s is instantaneous incoming solar radiation (W m^{-2}), R_{s24} is daily incoming solar radiation (MJ m^{-2} day), ρ_w is the density of water (kg m^{-3}), λ is the latent heat of vaporization for water (MJ kg^{-1}) and c is the numerical value of 1000, which is used to convert meters to millimeters.

Daily weighted footprints were required for comparison between daily ETa extrapolated and EC observations. A study conducted by Volk et al. (2023) proposed a protocol to create a daily weighted footprint based on hourly flux footprints. They recommended selecting hourly flux footprints in the range from 6:00 to 20:00 local time and a minimum of 5 hours of data per day. We selected hourly flux footprints when the incoming solar radiation values were above zero, footprint fetch values a minimum of 100 m, and flux footprints over vegetation.

3 Results and Discussion

3.1 Actual evapotranspiration (ETa) in turfgrass using the eddy covariance method

- **Energy balance closure of eddy-covariance measurements**

The surface energy balance before closure in 2021 and 2022 suggested that latent heat flux (LE) and sensible heat flux (H) over turfgrass were underestimated. The slope of the correlation between daily fluxes of Rn-G and LE+H was 0.8 and 0.9 in 2021 and 2022, respectively. These results concur with previous studies around the world, reporting apparent underestimation of turbulent heat fluxes (Mauder et al. 2020; Volk et al. 2023). Volk et al. (2023) analyzed 172 AmeriFlux EC stations and concluded that LE and H are underestimated by 14% and 10% respectively. Another study analyzed 50 FLUXNET sites and found a 21% underestimation of turbulent fluxes on average (Wilson et al. 2002). Instrument, and data processing errors, additional sources of energy, sub-mesoscale transport/ secondary circulations, and landscape heterogeneity in vegetation may be reasons for the surface energy balance closure problem (Stoy et al. 2013; Eshonkulov et al. 2019; Mauder et al. 2020). The discrepancies in the energy balance can be addressed by forcing closure. Figure 6 provides violin plots of EBC from the daily average per month. These values varied by month in

2021 and 2022. While in 2021, the highest EBC was observed in July, in 2022 the highest closure was obtained in June. However, the energy imbalance was lower in October 2021 and 2022. In general, monthly closure values ranged from 0.75-0.90. In summer, the spatial variability of the turfgrass was more evident and was quantified with an NDVI map (Fig. 12). In Figure 7, the different conditions for the energy flux measurements are visible as brown and green turfgrass around the EC tower and net radiometer, respectively. This difference in condition may explain the lower EBC in July and August. For instance, on July 27, 2022, the average hourly net radiation was 533.1 W/m2 and 595.0 W/m2 for brown and green turfgrass respectively. This would also effect the soil heat fluxes for these two patches. Previous studies have reported that instrumental errors and net radiation measurement problems are potential reasons for surface energy imbalance (Wilson et al. 2002; Foken 2008). Another explanation for the EBC gap may be the landscape-level heterogeneity (Stoy et al. 2013). Summer months showed high spatial variability across the golf course due to water supply and storage limitations.

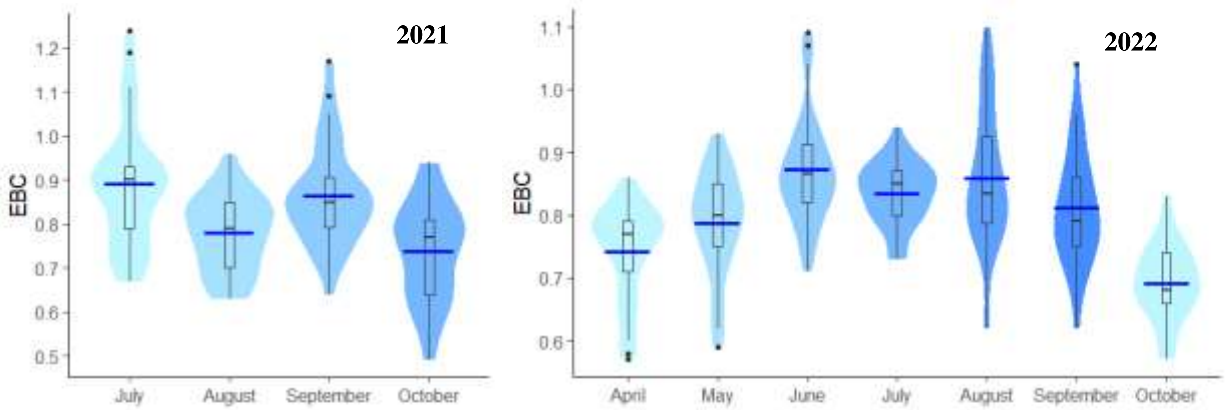

Fig 6. Daily energy balance closure in 2021 and 2022, the horizontal dark blue line shows the monthly average.

Fig 7. Aerial views of turfgrass and tree canopy on August 01, 2021, May 02, and July 27, 2022. The eddy covariance flux tower is marked with a red circle, the net radiometer and soil heat flux plates are marked with a yellow circle, and the predominant wind direction is marked with a blue arrow.

- **Daily actual evapotranspiration in urban turfgrass**

Figure 8 illustrates the daily ETa comparisons before and after the closure of ETa in 2021 and 2022. The daily ETa was high in May, June, July, August, and September and very low during April and October. The average of corrected daily ETa values was evaluated during the summer months of 2021 and 2022. The corrected daily ETa values in July and August in 2021 was slightly higher than in 2022 with values ranging from about 4.6 mm to 5.9 mm in 2021 and 4.6 mm to 5.0 mm in 2022. The higher values of daily ETa generally occurred in July when the days were warmer and dry. The total ET for July and August 2021 was 278.0 mm unforced, and 315.7 mm forced. The total ET for July and August 2022 was 252.5 mm unforced and 285.4 mm forced. The data set has some missing values for 2021 (3 red flags) and 2022 (9 red flags) due to precipitation events during those days.

In the literature, few studies have measured ETa using the EC method in urban turfgrass areas. In North Dakota, Niaghi et al. (2019) reported ETa for Kentucky bluegrass. The monthly average ETa was 4.7, 3.7, and 4.6 mm day^{-1} for July 2011, July 2012, and June 2013 respectively. In Florida, Jia et al. (2009) determined Kc and ETa for bahiagrass with the highest average monthly value of 4.22 mm day^{-1} occurring in May.

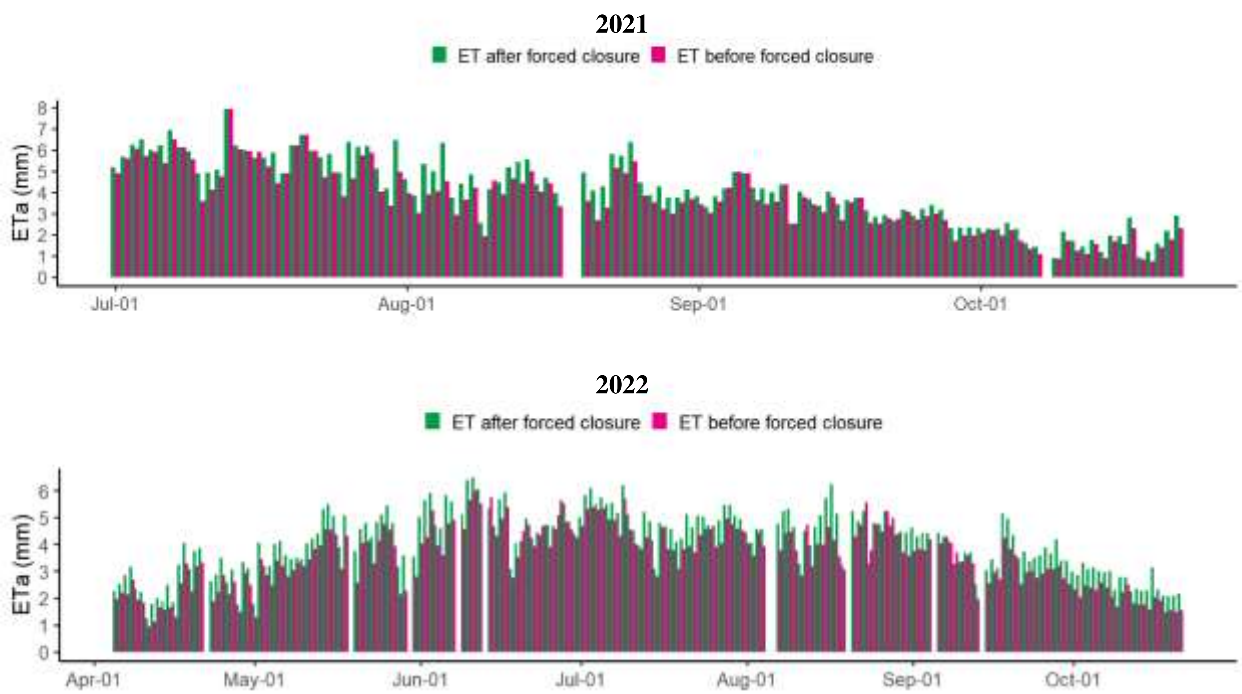

Fig 8. Daily comparisons before and after the forced closure of ETa amounts in 2021 and 2022.

3.2 Leaf Area Index in Turfgrass and Trees

The measured LAI in turfgrass ranged from 0.3 to 4.6, which included differing levels of turfgrass quality (low, intermediate, and high). The OSAVI, NDRE, NDVI, MSR, Ln(RVI), and EUR spectral vegetation indices were used to predict LAI in turfgrass. Figure 9 shows six LAI models, the “x” and “y” axes of which show the spectral vegetation indices selected and the measured LAI, respectively. The linear regression models were evaluated with R^2 and RSME, where R^2 ranged from 0.76 to 0.84, and RMSE ranged from 0.50 to 0.61 $cm^2\ cm^{-2}$. The SVIs EUR and MSR using the red-edge and NIR reflectance bands at 717 nm and 842 nm, respectively were found to be highly responsive to LAI in turfgrass and their high spatial resolution showed the best performance for LAI estimation with the highest R^2 and lowest RMSE. Previous research has shown the response of the red-edge and NIR bands provide more crucial information on leaf chlorophyll content (Dong et al. 2019) and fresh biomass amount (Verma et al., 2022) than other blue, green, and red reflectance bands. In this study, the high spatial resolution of UAS data has been recognized as a prospective approach for estimating LAI in turfgrass. Previous studies have shown the impact of high spatial resolution of remote sensing data on LAI estimation in crops (Du et al., 2022; Qi et al., 2020; Verma et al., 2022), and simultaneous changes in SVI associated with water content, leaf pigment, and canopy structure in urban turfgrass areas and trees under drought conditions (Miller et al. 2020).

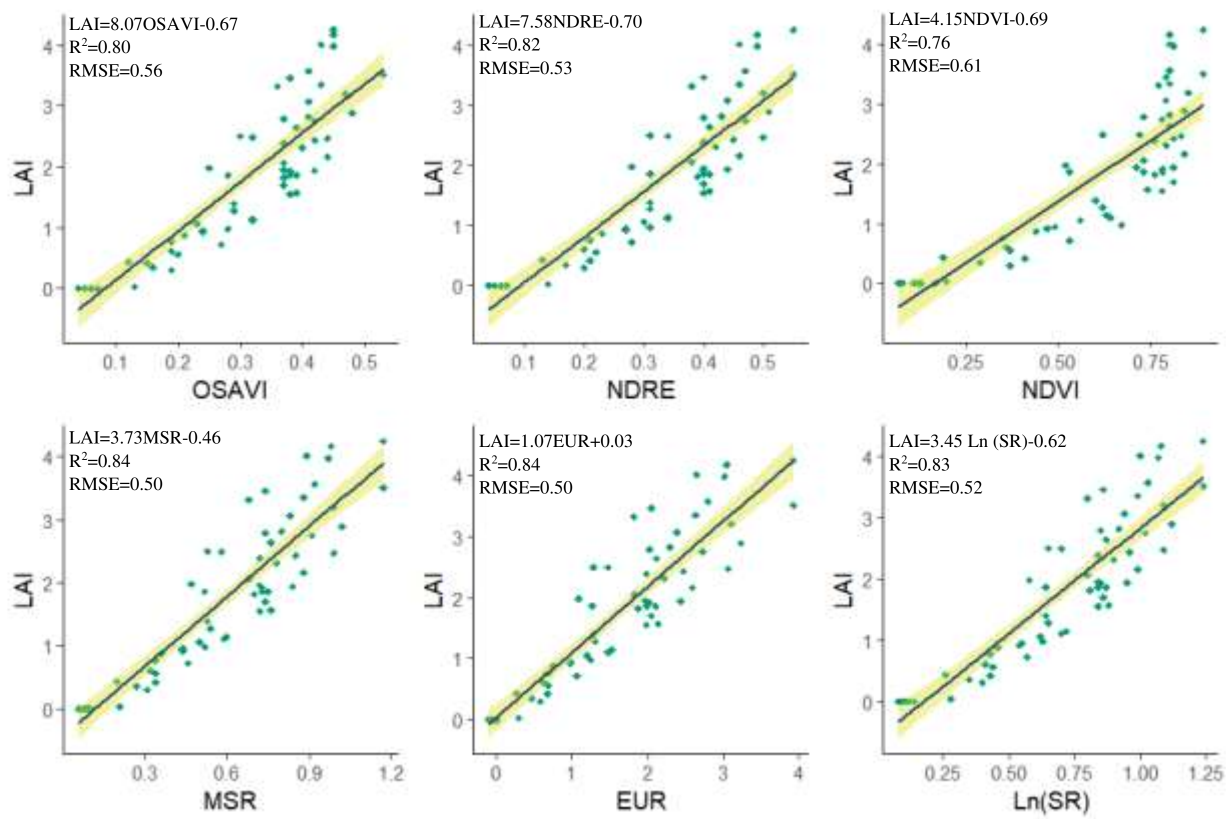

Fig 9. Comparisons between measured leaf area index and spectral vegetation indices with different regression models.

Trees represented 3% of the total area at the golf course, so 13 isolated trees were selected randomly to measure LAI, most of which were coniferous species. The measurements below the canopy were at a distance from 0.5 m to 1 m and a height of 0.95 cm. Our approach also agreed with Wei et al. (2020), who reported good accuracy of LAI values using an LAI 2200 C plant canopy analyzer at a similar sensor position. Crown shape information is relevant for the estimation of LAI of isolated trees and requires a simple, cost-effective, and portable device to generate a crown shape (Wei et al. 2020). 3D reconstruction using sUAS was used to generate crown profiles and improve LAI estimations (Fig.17 in Appendix). The selected isolated trees had heights from 5.1 m to 17 m, with a mean value of 12 m. The LAI mostly falls between 2.2 and 4.3, similar to Xing et al. (2019). Other studies reported that LAI measurements made with the LAI 2200 C sensor were consistent and accurate when LAI was less than 5 (Wei et al. 2020).

3.3 Two Source energy balance and eddy covariance comparison

This section presents an assessment of the TSEB model combining sUAS imagery, an LAI model, hourly flux footprints, daily ET scalar extrapolation techniques, and daily flux footprints to accurately model urban turfgrass ETa at hourly and daily scales.

- **Land surface temperature, Leaf area index (LAI), Fractional cover (f_c) and Green ground cover (f_g)**

Figure 10 shows an example of LAI, LST, $f_{c,}$ and f_g rasters for the TSEB model. High spatial resolution UAS allows for distinguishing small-scale heterogeneity. An LAI map was created using the EUR vegetation index. This map shows the LAI range from 0 to 4.3, where LAI equal to zero corresponds to impervious surfaces, LAI in the range $0 < \text{LAI} < 4.3$ is turfgrass and LAI ~4.3 corresponds to trees. The landscape type and LAI are a good indicators of ET (Saher et al. 2022) with R^2 ranging from 0.43 to 0.87 (Wei et al. 2017). However, unreliable estimations of LAI may create uncertainties on model results and a 0.1 m^2/m^2 change in LAI is associated with a 3% change in simulated H with TSEB (Burchard-Levine et al. 2020).

The LST map shows warm and cold areas. The lowest LST values were observed for actively growing turfgrass, trees, and reservoirs surfaces. In contrast, the highest LST values were observed for buildings and dormant turfgrass. As pointed out by Wang et al. (2018), LST is decreased by increasing tree cover, tree density, LAI, and water covers in urban parks. This is because green urban surfaces shade and absorb radiation energy via transpiration and photosynthesis which decreases LST. For example, irrigated turfgrass, trees, and shrubs have an efficient cooling effect in urban parks in Salt Lake (Gómez-Navarro et al. 2021) , Las Vegas, and Phoenix (Saher et al. 2022). TSEB model results were more sensitive to LST compared to LAI, where 1K change is associated with ~12-25 W m^{-2} (Gan and Gao 2015; Burchard-Levine et al. 2020).

The fractional cover map shows the areas of vegetation and non-vegetation, with the highest values of f_c observed in turfgrass and tree areas. The green fractional cover map shows a range from 0 to 0.9. This map reflects the range of highest values for active transpiration and photosynthesis. These biophysical variables have an important role in turfgrass – tree ecosystem energy fluxes, of which fractional cover was the most influential parameter on the TSEB model performance (Burchard-Levine et al. 2020). Of the different predictors, NDVI was relevant for modeling ET of urban vegetation such as trees and turfgrass (Nouri et al. 2013; Vulova et al. 2021).

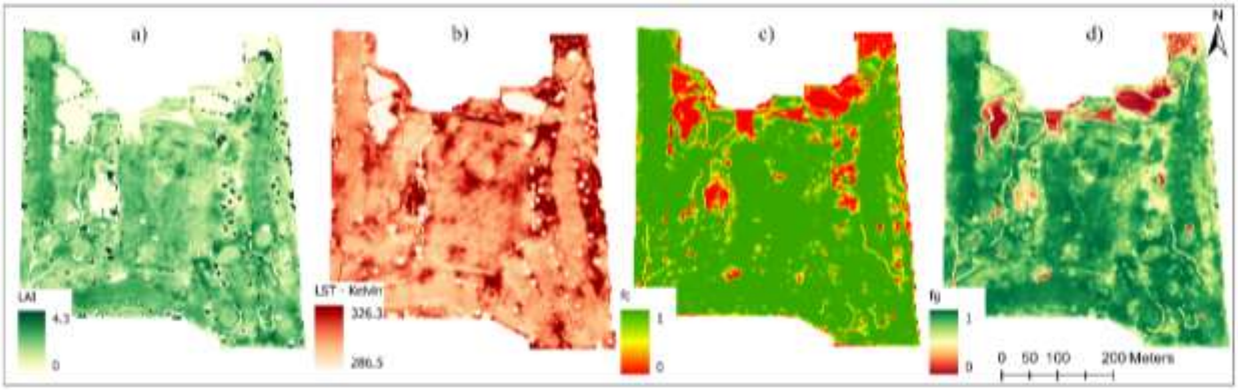

Fig 10. Example of raster inputs for TSEB-PT model. a) Leaf area index, b) land surface temperature, c) fractional cover, and d) green ground cover at the 3m resolution on May 18, 2022.

- **Assessing the Hourly TSEB - PT versus EC Measurements**

Hourly energy fluxes were modeled for turfgrass and trees by the TSEB-PT model at 3 m resolution using the aggregated UAS-based remotely sensed observations. Figure 11 shows the energy flux maps for the study area on May 18, 2022.

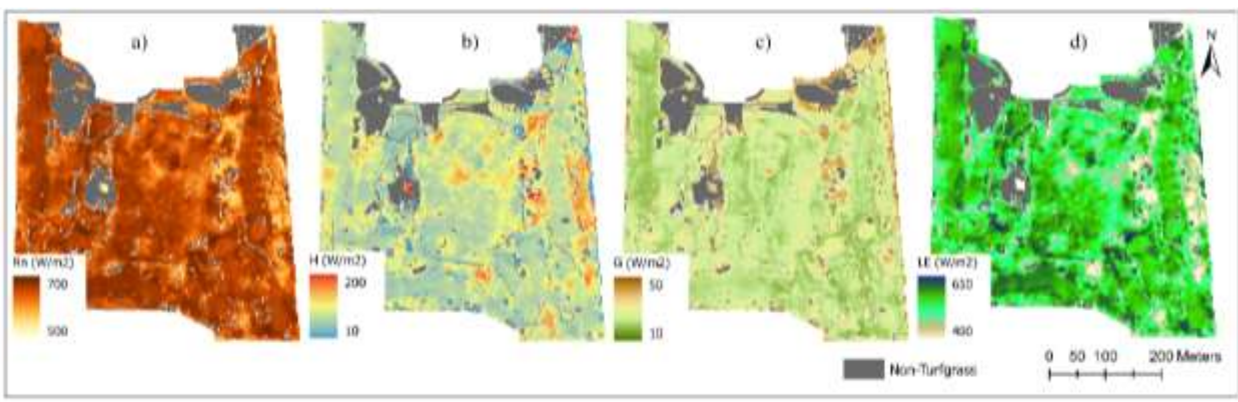

Fig 11. Net radiation, sensible heat flux, latent heat flux, and ground heat flux map on May 18, 2022

A two-dimensional flux footprint model was used to compute footprint-weighted aggregated model outputs for comparison of TSEB-PT results with EC data. Figure 12 illustrates the footprint source areas for the flight dates in October 2021, May 2022, and July 2022. The footprint fetch (blue lines) identifies the maximum distance between the EC tower and the extent of the source area. The orientation and dimensions of the flux footprint depended on the height of the instrumentation, surface roughness length, wind speed and direction, and atmospheric stability (Chen et al. 2009), as shown in Table 6 in the Appendix. It can be seen that the flux footprint fetch in October 2021 was higher than in May 2022 and July 2022. This change is attributed to the reduction in the sensor height from 2.6 m in 2021 to 2 m in 2022. In order to get a footprint of the homogenous turfgrass area, the location and height of the instrumentation must be considered due to high spatial variability (turfgrass, trees, sand traps, sidewalks, reservoirs, etc).

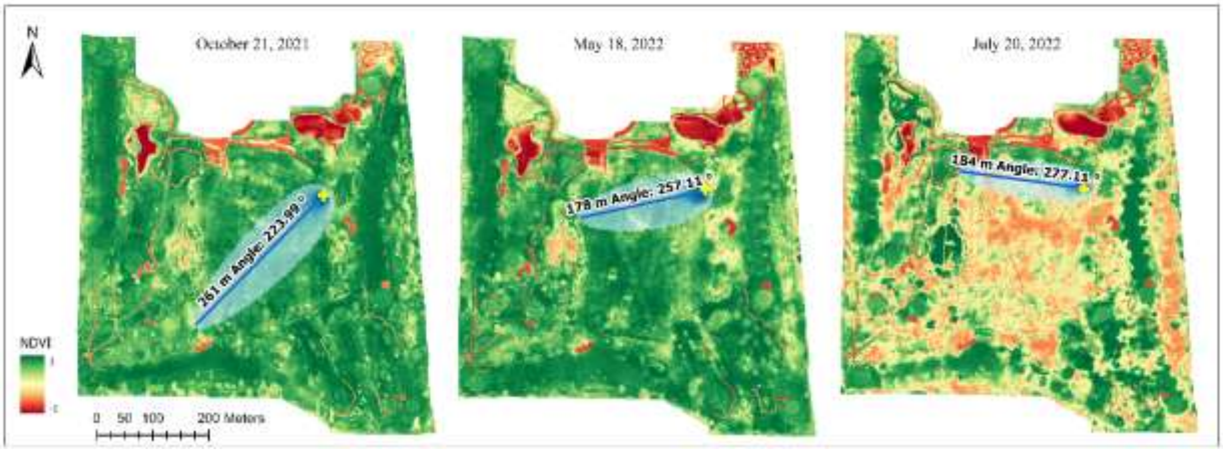

Fig 12. Maps of hourly flux footprint at the golf course. In each panel, an NDVI map with an eddy covariance flux tower (marked with a yellow cross) was overlaid with an hourly flux footprint. Blue lines denote the distance and angle of the flux footprint fetch.

To assess the utility of the TSEB-PT model, hourly modeled fluxes were compared with EC measurements both closed and unclosed. Figure 13 illustrates five comparisons that were made between the surface energy fluxes modeled using the TSEB-PT and field measurements from the EC for non-closed and closed energy balance. In Table 4, the performance of the TSEB model for each energy flux component is associated with the statistical metric MAE, RMSE, and RMSE for both EC closed and unclosed fluxes within the footprint. We found a strong R^2 of 0.95 and RMSE for Rn estimates of 32 W m^{-2}. According to other studies (Nassar et al. 2021; Simpson et al. 2021; Burchard-Levine et al. 2021; Gao et al. 2022), TSEB estimates of R_n have good agreement with measurements. High-resolution imagery (< 5 m) allows for the discrimination between grass and tree pixels and achieves better accuracy of estimated ET with RMSE ~50 Wm^{-2} (Burchard-Levine et al., 2021b). The EC-TSEB agreement in H and LE with forced closure has RMSE values of 35 W m^{-2} and 50 W m^{-2} respectively, which is considered acceptable and similar to prior studies (e.g., Aboutalebi et al. 2019b; Burchard-Levine et al. 2021; Simpson et al. 2022). On July 20, 2022, there is an H overestimation of nearly 65 Wm^{-2} due to a lack of uniform green turfgrass within the footprint. Figure 12 shows that the average NDVI was equal to 0.3 within the footprint, which explains the present of dead turfgrass on July 20, 2022. In a natural ecosystem, an overestimation of H was found when the area included soil and tree surfaces (Burchard-Levine et al. 2021).

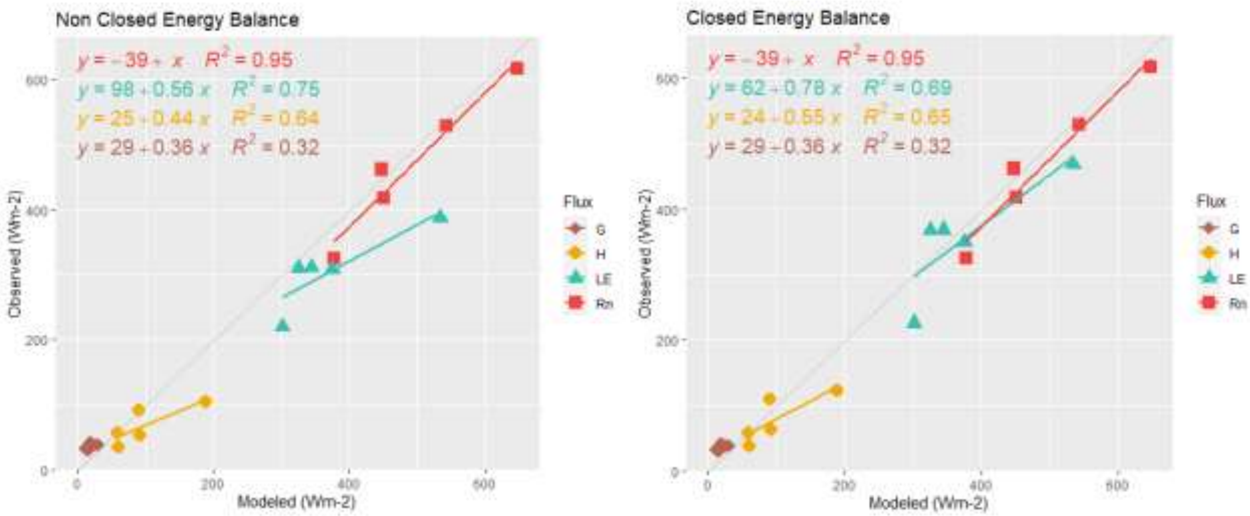

Fig 13. Energy flux comparisons using uncorrected EC station (observed) and UAS-derived (modeled) data.

Table 4. Performance of the TSEB model for non closed and closed energy balance (units in W m^{-2}).

	Variable	MAE	RMSE	RRMSE
	Rn	29	32	7
	G	17	18	48
Non Closed	H	31	43	64
	LE	68	82	27
Closed	H	28	35	44
	LE	46	50	14

Modeled urban ET has been reported using integrated SEB models, remote sensing, and spectral vegetation indices (Vulova Stenka et al. 2018; Nouri et al. 2020; Feng et al. 2022). However, ET models may be verify using instrumentation to measure ETa (Feng et al. 2022). Recently urban ET studies have used remote sensing, GIS, flux modeling, artificial intelligence, and meteorological data (Vulova et al. 2021). In this research, modeling ETa in golf courses was required for developing decision support system tools (Carlson et al. 2022). The TSEB-PT model was tested in an urban turfgrass area at a golf course in Utah, at the local scale (20 hectares).

- **Solar radiation scaling model (RS) and observed daily actual evapotranspiration**

The remote ETa estimates acquired with sUAS are near instantaneous data during the day and have to be upscaled to daily total ETa to become useful for water managers (Cammalleri et al. 2014). This is because EC measurements may provide spatial ET values within the flux footprint but not for the entire golf course. The solar radiation scaling model (RS) was suggested as a robust method for daytime upscaling of ET in heterogeneous natural landscapes (Awada et al. 2021), vineyards (Semmens et al. 2016; Nassar et al. 2021), croplands, and grasslands (Chávez et al. 2008; Cammalleri et al. 2014; Xu et al. 2015). In this study, the RS method was applied, and the daily flux footprint model was computed (Fig.14) for the comparison between the extrapolated daily ET (UAS-ET) and directly measured ETa values (Table 5). The difference between the daily ET from TSEB versus measured with closure varied from 0.54 to 0.84 mm day^{-1} with RMSE a 0.6 mm day^{-1}. This result agrees with the magnitude of RMSE from 0.37 to 0.79 mm day^{-1} in corn and soybean fields (Chávez et al. 2008). Other studies reported an RMSE of 0.58 mm day^{-1} in wheat, maize, and corn (Xu et al. 2015); and ~0.5 mm day^{-1} in vineyards (Semmens et al. 2016; Nassar et al. 2021).

Fig 14. Contour maps of daily flux footprint at the golf course. In each panel, a false color map with an eddy covariance flux tower (marked with a yellow cross) was overlaid with a daily flux footprint.

Table 5. Daily evapotranspiration from scaling model (RS) and eddy covariance measurements (EC), and root mean square error (RMSE) (units in mm day^{-1})

Date	DOY	ET_d		RMSE
		RS	EC	
21-Oct-21	294	2.7	2.2	0.6
18-May-22	138	6.1	5.3	
20-Jul-22	201	3.4	4.1	
19-Sep-22	262	3.8	4.3	

4 Conclusions

Urban turfgrass evapotranspiration plays an important role in irrigation water management but ET is difficult to measure and estimate in urban landscapes due to large spatial variability in land cover and land use. This study demonstrated the application of the Two-Source Energy Balance model using the Priestley-Taylor approach (TSEB - PT) and sUAS imagery data for deriving gridded ETa estimates for urban turfgrass, which was validated with EC measurements. Results from EC measurements and the energy balance closure (Bowen Ratio) showed that the ETa average for urban turfgrass in drought summer ranged from about 4.6 mm to 5.9 mm in 2021 and 5.2 mm to 5.6 mm in 2022.

The LAIs of turfgrass and isolated trees were used to model ETa. Utilizing high-resolution multispectral imagery collected from a sUAS, we demonstrated the potential for using near infrared and red edge reflectance-based spectral vegetation indices such as OSAVI, NDRE, NDVI, MSR, EUR, and Ln(NIR/Red Edge) to establish a LAI empirical model applicable to urban turfgrass. The linear regression model had the highest accuracy for LAI estimation with R^2 ranging from 0.76 to 0.84 and the lowest RMSE ranging from

0.5 to 0.6. However, 3D reconstruction using sUAS point cloud data was useful for post-processing LAI of isolated coniferous trees, showing the LAI in trees mostly falls between the range of 2.2 and 4.3.

The high-resolution multispectral and thermal imagery collected from UAS around solar noon, the LAI protocol development, supervised classification of land use/cover, and thermal band calibration gave reliable estimates of energy fluxes for urban turfgrass and trees. The TSEB –PT model validation and energy balance closure results showed that latent and sensible heat flux retrievals were accurate with an overall RMSE of ~50.5 W m^{-2}.

The RS-ET estimations were extrapolated from hourly to daily values yielding a RMSE of 0.6 mm day^{-1}. This study highlights the ability of the TSEB-PT model using sUAS imagery to estimate the spatial variation of daily ETa for an urban turfgrass surface, which is useful for landscape irrigation management in arid and semi-arid areas. The UAS-ET spatial map is a support tool for implementing precision irrigation and irrigation scheduling at field scale. In addition, ET (latent heat flux) spatial maps of urban turfgrass may useful in determining large scale energy balances in urban environments.

5 Acknowledgment

This study was possible thanks to support from Utah Water Research Laboratory Student Fellowship and the United States Golf Association. The authors are also grateful for the extraordinary support from the Utah State University AggieAir sUAS program staff and Agricola Research team for data collection support and analysis. Mention of trade names or commercial products in this publication is solely for the purpose of providing specific information and does not imply recommendation or endorsement by the U.S. Department of Agriculture. USDA is an equal opportunity provider and employer.

6 Appendix

Fig 15. a) High, b) intermediate, and c) low turfgrass quality for sampling leaves.

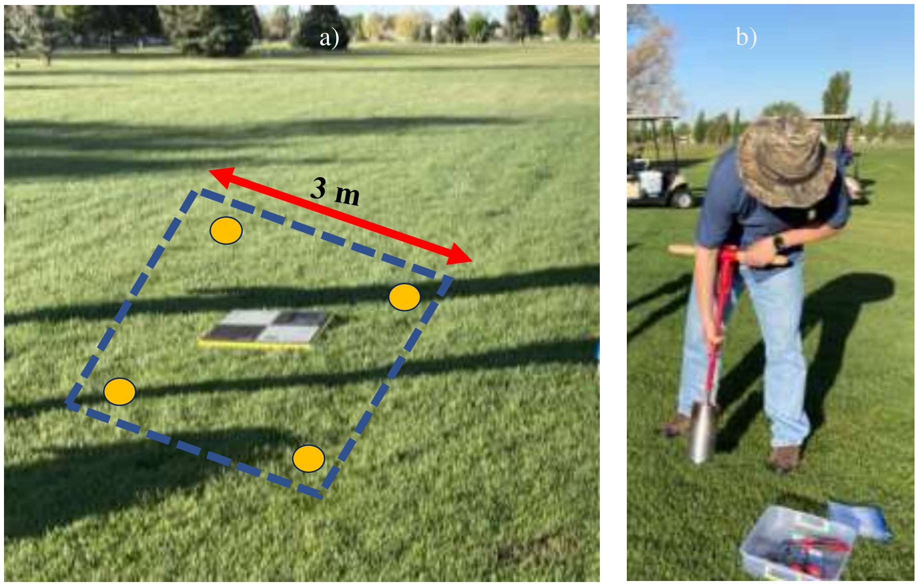

Fig 16. a) A sampling location with four replications and b) sampling turfgrass with a turfgrass cup cutter.

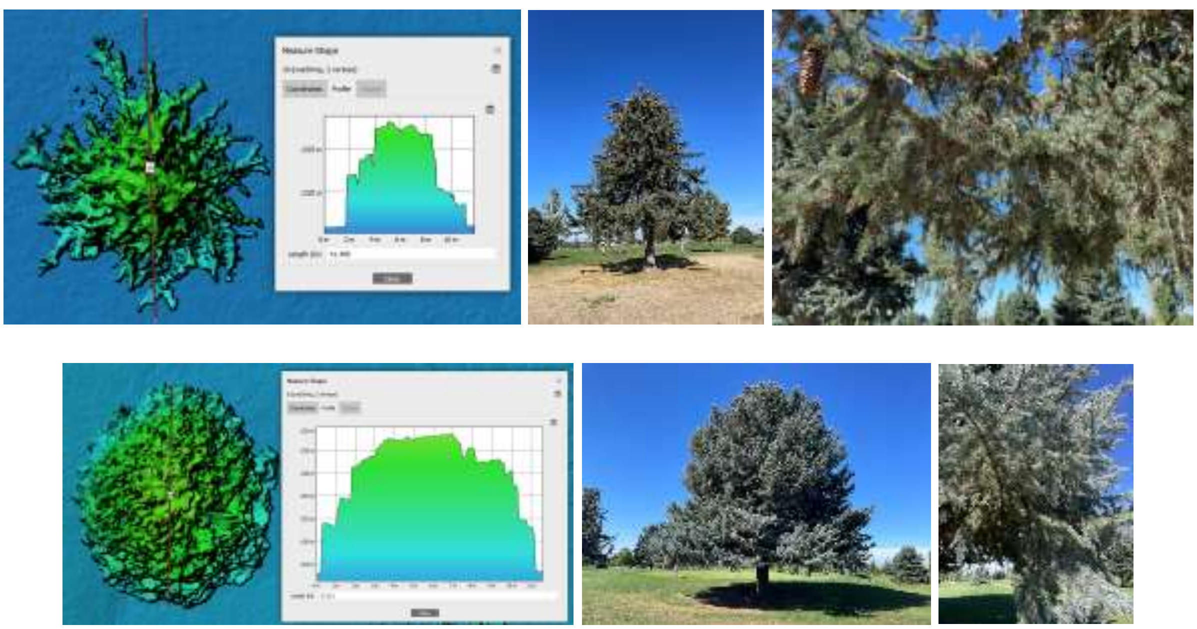

Fig 17. Crow profile from a 3D reconstruction using sUAS point cloud data.

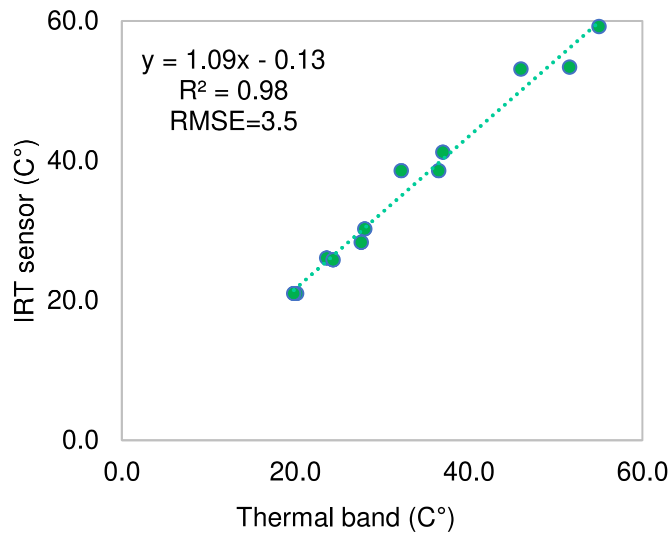

Fig 18. Linear regression of thermal band calibration using infrared thermometer sensors (IRTs).

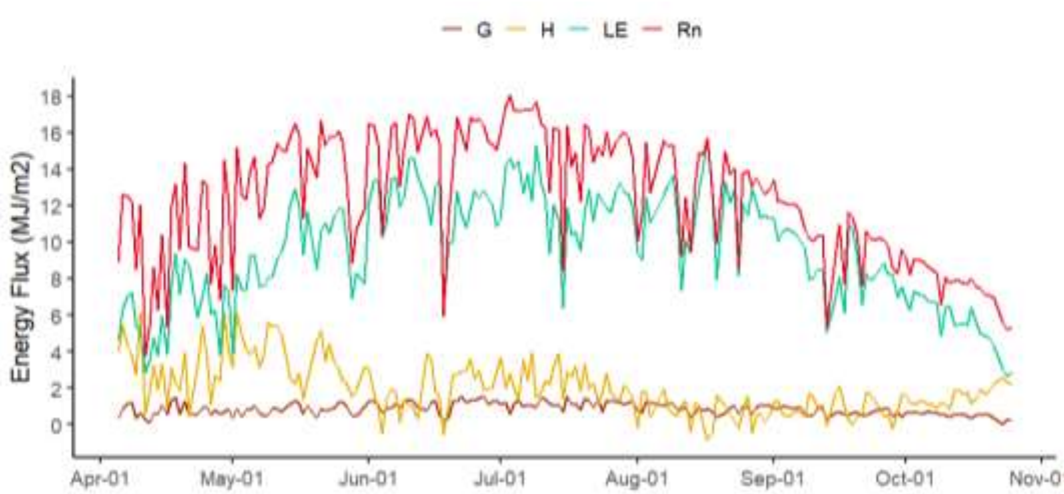

Fig 19. Time series of net radiation (Rn), sensible heat flux (H), latent heat flux (LE), and ground heat flux (G) from closed energy balance in 2022.

Table 6. Inputs required for deriving an hourly flux footprint model.

Date	Time	Wind Dir	umean (m s-1)	ustar (m s-1)	L (m)	zm (m)	z0 (m)	Sigmav (m s-1)
21-Oct-21	13:00 -14:00 pm	224	1.7	0.2	-10.2	2.6	0.01	0.70
18-May-22	13:00 -14:00 pm	257	2.1	0.2	-7.3	2.0	0.01	0.72
20-Jul-22	14:00 -15:00 pm	277	1.4	0.2	-6.1	2.0	0.01	0.68

wind_dir=Vector of wind direction in degrees (of 360) for rotation of the footprint, umean=Vector of mean wind speed, ustar= Vector of friction velocity, L = Vector of Obukhov length, zm = Measurement height above displacement height, z0 =Roughness length, sigmav=Vector of standard deviation of lateral velocity fluctuations.

7 References

Aboutalebi M, Torres-Rua AF, Kustas WP, et al (2019a) Assessment of different methods for shadow detection in high-resolution optical imagery and evaluation of shadow impact on calculation of NDVI, and evapotranspiration. Irrig Sci 37:407–429. https://doi.org/10.1007/s00271-018-0613-9

Aboutalebi M, Torres-Rua AF, Kustas WP, et al (2019b) Assessment of different methods for shadow detection in high-resolution optical imagery and evaluation of shadow impact on calculation of NDVI, and evapotranspiration. Irrig Sci 37:407–429. https://doi.org/10.1007/s00271-018-0613-9

Aboutalebi M, Torres-Rua AF, McKee M, et al (2022) Downscaling UAV land surface temperature using a coupled wavelet-machine learning-optimization algorithm and its impact on evapotranspiration. Irrig Sci 40:553–574. https://doi.org/10.1007/s00271-022-00801-2

Agam N, Kustas WP, Anderson MC, et al (2010) Application of the priestley-taylor approach in a two-source surface energy balance model. J Hydrometeorol 11:185–198. https://doi.org/10.1175/2009JHM1124.1

Awada H, di Prima S, Sirca C, et al (2021) Daily actual evapotranspiration estimation in a mediterranean ecosystem from landsat observations using SEBAL approach. Forests 12:1–20. https://doi.org/10.3390/f12020189

Badzmierowski MJ, McCall DS, Evanylo G (2019) Using hyperspectral and multispectral indices to detect water stress for an urban turfgrass system. Agronomy 9:. https://doi.org/10.3390/agronomy9080439

Braun RC, Bremer DJ, Ebdon JS, et al (2022a) Review of cool-season turfgrass water use and requirements: II. Responses to drought stress. Crop Sci 62:1685–1701

Braun RC, Bremer DJ, Ebdon JS, et al (2022b) Review of cool-season turfgrass water use and requirements: I. Evapotranspiration and responses to deficit irrigation. Crop Sci 62:1661–1684. https://doi.org/10.1002/csc2.20791

Brewer K, Clulow A, Sibanda M, et al (2022) Estimation of Maize Foliar Temperature and Stomatal Conductance as Indicators of Water Stress Based on Optical and Thermal Imagery Acquired Using an Unmanned Aerial Vehicle (UAV) Platform. Drones 6:. https://doi.org/10.3390/drones6070169

Burchard-Levine V, Nieto H, Riaño D, et al (2021) The effect of pixel heterogeneity for remote sensing based retrievals of evapotranspiration in a semi-arid tree-grass ecosystem. Remote Sens Environ 260:. https://doi.org/10.1016/j.rse.2021.112440

Burchard-Levine V, Nieto H, Riaño D, et al (2020) Seasonal adaptation of the thermal-based two-source energy balance model for estimating evapotranspiration in a semiarid tree-grass ecosystem. Remote Sens (Basel) 12:. https://doi.org/10.3390/rs12060904

Cammalleri C, Anderson MC, Kustas WP (2014) Upscaling of evapotranspiration fluxes from instantaneous to daytime scales for thermal remote sensing applications. Hydrol Earth Syst Sci 18:1885–1894. https://doi.org/10.5194/hess-18-1885-2014

Campbell GS, Norman JM (1998) An Introduction to Environmental Biophysics. Springer New York

Carlson MG, Gaussoin RE, Puntel LA (2022) A review of precision management for golf course turfgrass. Crop, Forage & Turfgrass Management 8:. https://doi.org/10.1002/cft2.20183

Chávez JL, Neale CMU, Prueger JH, Kustas WP (2008) Daily evapotranspiration estimates from extrapolating instantaneous airborne remote sensing et values. Irrig Sci 27:67–81. https://doi.org/10.1007/s00271-008-0122-3

Chen B, Black TA, Coops NC, et al (2009) Assessing tower flux footprint climatology and scaling between remotely sensed and eddy covariance measurements. Boundary Layer Meteorol 130:137–167. https://doi.org/10.1007/s10546-008-9339-1

Cheng J, Kustas WP (2019) Using very high resolution thermal infrared imagery for more accurate determination of the impact of land cover differences on evapotranspiration in an irrigated agricultural area. Remote Sens (Basel) 11:. https://doi.org/10.3390/rs11060613

Colaizzi PD, Evett SR, Howell TA, et al (2006) Comparison of Five Models to Scale Daily Evapotranspiration from One-Time-of-Day Measurements. Transactions of the ASABE 49:1409–1417

Cuxart J, Boone AA (2020) Evapotranspiration over Land from a Boundary-Layer Meteorology Perspective. Boundary Layer Meteorol 177:427–459. https://doi.org/10.1007/s10546-020-00550-9

Dong T, Liu J, Shang J, et al (2019) Assessment of red-edge vegetation indices for crop leaf area index estimation. Remote Sens Environ 222:133–143. https://doi.org/10.1016/j.rse.2018.12.032

Du L, Yang H, Song X, et al (2022) Estimating leaf area index of maize using UAV-based digital imagery and machine learning methods. Sci Rep 12:. https://doi.org/10.1038/s41598-022-20299-0

Eshonkulov R, Poyda A, Ingwersen J, et al (2019) Evaluating multi-year, multi-site data on the energy balance closure of eddy-covariance flux measurements at cropland sites in southwestern Germany. Biogeosciences 16:521–540. https://doi.org/10.5194/bg-16-521-2019

Feng J, Wang W, Che T, Xu F (2023) Performance of the improved two-source energy balance model for estimating evapotranspiration over the heterogeneous surface. Agric Water Manag 278:108159. https://doi.org/10.1016/j.agwat.2023.108159

Feng L, Liu Y, Zhou Y, Yang S (2022) A UAV-derived thermal infrared remote sensing three-temperature model and estimation of various vegetation evapotranspiration in urban micro-environments. Urban For Urban Green 69:. https://doi.org/10.1016/j.ufug.2022.127495

Finley SL, Basu NB (2020) Curbing the Summer Surge: Permanent Outdoor Water Use Restrictions in Humid and Semiarid Cities. Water Resour Res 56:. https://doi.org/10.1029/2019WR026466

Foken T (2008) The energy balance closure problem: An overview. Ecological Applications 18:1351–1367. https://doi.org/10.1890/06-0922.1

French AN, Schmugge TJ, Kustas WP, et al (2003) Surface energy fluxes over El Reno, Oklahoma, using high-resolution remotely sensed data. Water Resour Res 39

Gan G, Gao Y (2015) Estimating time series of land surface energy fluxes using optimized two source energy balance schemes: Model formulation, calibration, and validation. Agric For Meteorol 208:62–75. https://doi.org/10.1016/j.agrformet.2015.04.007

Gao R, Nassar A, Torres-Rua AF (2021) Footprint area generating based on eddy covariance records. In: HydroShare. https://doi.org/10.4211/hs.eb6eeeccdbe546fc941f3c219cb05a34. Accessed 1 Jun 2022

Gao R, Torres-Rua AF, Aboutalebi M, et al (2022) LAI estimation across California vineyards using sUAS multi-seasonal multi-spectral, thermal, and elevation information and machine learning. Irrig Sci. https://doi.org/10.1007/s00271-022-00776-0

Gao R, Torres-Rua AF, Nieto H, et al (2023) ET Partitioning Assessment Using the TSEB Model and sUAS Information across California Central Valley Vineyards. Remote Sens (Basel) 15:. https://doi.org/10.3390/rs15030756

García-Santos V, Sánchez JM, Cuxart J (2022) Evapotranspiration Acquired with Remote Sensing Thermal-Based Algorithms: A State-of-the-Art Review. Remote Sens (Basel) 14

Gelernter WD, Stowell LJ, Johnson ME, et al (2015) Documenting Trends in Water Use and Conservation Practices on U.S. Golf Courses. Crop, Forage & Turfgrass Management 1:1–10. https://doi.org/10.2134/cftm2015.0149

Gómez-Navarro C, Pataki DE, Pardyjak ER, Bowling DR (2021) Effects of vegetation on the spatial and temporal variation of microclimate in the urbanized Salt Lake Valley. Agric For Meteorol 296:. https://doi.org/10.1016/j.agrformet.2020.108211

Gutman G, Ignatov A (1998) The derivation of the green vegetation fraction from NOAA/AVHRR data for use in numerical weather prediction models. Int J Remote Sens 19:1533–1543. https://doi.org/10.1080/014311698215333

Hartling S, Sagan V, Maimaitijiang M (2021) Urban tree species classification using UAV-based multi-sensor data fusion and machine learning. GIsci Remote Sens 58:1250–1275. https://doi.org/10.1080/15481603.2021.1974275

Hassler SC, Baysal-Gurel F (2019) Unmanned aircraft system (UAS) technology and applications in agriculture. Agronomy 9

Hong M, Bremer DJ, van der Merwe D (2019) Thermal Imaging Detects Early Drought Stress in Turfgrass Utilizing Small Unmanned Aircraft Systems. Agrosystems, Geosciences and Environment 2:1–9. https://doi.org/10.2134/age2019.04.0028

Jackson RD, Hatfield JL, Reginato R (1983) Estimation of Daily Evapotranspiration from One Time-of-Day Measurements. Agric Water Manag 7:351–362

Jia X, Dukes MD, Jacobs JM (2009) Bahiagrass crop coefficients from eddy correlation measurements in central Florida. Irrig Sci 28:5–15. https://doi.org/10.1007/s00271-009-0176-x

K Webb BE, Pearman GI, Leuning R (1980) Correction of flux measurements for density effects due to heat and water vapour transfer. Meteor Soc 106:85–100

Katz L, Ben-Gal A, Litaor MI, et al (2022) A spatiotemporal decision support protocol based on thermal imagery for variable rate drip irrigation of a peach orchard. Irrig Sci. https://doi.org/10.1007/s00271-022-00830-x

Kljun N, Calanca P, Rotach MW, Schmid HP (2015) A simple two-dimensional parameterisation for Flux Footprint Prediction (FFP). Geosci Model Dev 8:3695–3713. https://doi.org/10.5194/gmd-8-3695-2015

Kumar Yadav P, Alex Thomasson J, Hardin R, et al (2023) Detecting volunteer cotton plants in a corn field with deep learning on UAV remote-sensing imagery. Comput Electron Agric 204:107551. https://doi.org/10.1016/j.compag.2022.107551

Kustas WP, Alfieri JG, Nieto H, et al (2019) Utility of the two-source energy balance (TSEB) model in vine and interrow flux partitioning over the growing season. Irrig Sci 37:375–388. https://doi.org/10.1007/s00271-018-0586-8

Kustas WP, Norman JM (1999) Evaluation of soil and vegetation heat ¯ux predictions using a simple two-source model with radiometric temperatures for partial canopy cover

Lee G, Kim G, Min G, et al (2023) Vegetation Classification in Urban Areas by Combining UAV-Based NDVI and Thermal Infrared Image. Applied Sciences (Switzerland) 13:. https://doi.org/10.3390/app13010515

Litvak E, Pataki DE (2016) Evapotranspiration of urban lawns in a semi-arid environment: An in situ evaluation of microclimatic conditions and watering recommendations. J Arid Environ 134:87–96. https://doi.org/10.1016/j.jaridenv.2016.06.016

Liu Wenjuan, Hong Yang, Khan Sadiq Ibrahim, et al (2010) Actual evapotranspiration estimation for different land use and land cover in urban regions using Landsat 5 data. J Appl Remote Sens 4:041873. https://doi.org/10.1117/1.3525566

Lu S, Xuan J, Zhang T, et al (2022) Effect of the Shadow Pixels on Evapotranspiration Inversion of Vineyard: A High-Resolution UAV-Based and Ground-Based Remote Sensing Measurements. Remote Sens (Basel) 14:. https://doi.org/10.3390/rs14092259

Maas J, van Dillen SME, Verheij RA, Groenewegen PP (2009) Social contacts as a possible mechanism behind the relation between green space and health. Health Place 15:586–595. https://doi.org/10.1016/j.healthplace.2008.09.006

Marín J, Yousfi S, Mauri P v., et al (2020) RGB vegetation indices, NDVI, and biomass as indicators to evaluate C3 and C4 turfgrass under differentwater conditions. Sustainability (Switzerland) 12:. https://doi.org/10.3390/su12062160

Massman WJ, Lee X (2002) Eddy covariance flux corrections and uncertainties in long-term studies of carbon and energy exchanges

Mauder M, Foken T, Cuxart J (2020) Surface-Energy-Balance Closure over Land: A Review. Boundary Layer Meteorol 177:395–426. https://doi.org/10.1007/s10546-020-00529-6

Maupin MA, J.F. Kenny, S.S. Hutson, et al (2022) Landscape Irrigation and Water Conservation in Urban Areas: An Analysis of Information-based Strategies. Horttechnology 32:213–225. https://doi.org/10.21273/HORTTECH05001-21

Mauri PV, Yousfi S, Parra L, et al (2022) The Usefulness of Drone Imagery and Remote Sensing Methods for Monitoring Turfgrass Irrigation. In: Kacprzyk J, Balas VE, Ezziyyani M (eds) Advanced Intelligent Systems for Sustainable Development (AI2SD'2020). Springer International Publishing, Cham, pp 913–923

McNaughton KG, Van Den Hurk BJJM (1995) A 'Lagrangian' revision of the resistors in the two-layer model for calculating the energy budget of a plant canopy. Boundary Layer Meteorol 74:261–288. https://doi.org/10.1007/BF00712121

Meza K, Torres-Rua A, Hipps L, et al (2023) Protocol for Measuring Leaf Area Index (LAI) in Urban Turfgrass Using a Destructive Method. In: HydroShare. http://www.hydroshare.org/resource/1940e04333584dada3f1d5fed4bee15b. Accessed 20 May 2023

Milas AS, Arend K, Mayer C, et al (2017) Different colours of shadows: classification of UAV images. Int J Remote Sens 38:3084–3100. https://doi.org/10.1080/01431161.2016.1274449

Miller DL, Alonzo M, Roberts DA, et al (2020) Drought response of urban trees and turfgrass using airborne imaging spectroscopy. Remote Sens Environ 240:. https://doi.org/10.1016/j.rse.2020.111646

Mokhtari A, Ahmadi A, Daccache A, Drechsler K (2021) Actual evapotranspiration from UAV images: A multi-sensor data fusion approach. Remote Sens (Basel) 13:. https://doi.org/10.3390/rs13122315

Nagler PL, Scott RL, Westenburg C, et al (2005) Evapotranspiration on western U.S. rivers estimated using the Enhanced Vegetation Index from MODIS and data from eddy covariance and Bowen ratio flux towers. Remote Sens Environ 97:337–351. https://doi.org/10.1016/j.rse.2005.05.011

Nassar A, Torres-Rua A, Hipps L, et al (2022) Using Remote Sensing to Estimate Scales of Spatial Heterogeneity to Analyze Evapotranspiration Modeling in a Natural Ecosystem. Remote Sens (Basel) 14:. https://doi.org/10.3390/rs14020372

Nassar A, Torres-rua A, Kustas W, et al (2021) Assessing Daily Evapotranspiration Methodologies from One-Time-of-Day sUAS and EC Information in the GRAPEX Project. Remote Sens (Basel) 13:. https://doi.org/10.3390/rs13152887

Niaghi AR, Jia X, Scherer T, Steele D (2019) Measurement of Unirrigated Turfgrass Evapotranspiration Rate in the Red River Valley. Vadose Zone Journal 18:1–11. https://doi.org/10.2136/vzj2018.11.0202

Nieto H, Kustas WP, Torres-Rúa A, et al (2019) Evaluation of TSEB turbulent fluxes using different methods for the retrieval of soil and canopy component temperatures from UAV thermal and multispectral imagery. Irrig Sci 37:389–406. https://doi.org/10.1007/s00271-018-0585-9

Niu H, Hollenbeck D, Zhao T, et al (2020) Evapotranspiration estimation with small uavs in precision agriculture. Sensors (Switzerland) 20:1–28

Norman JM, Kustas WP, Humes KS (1995) Source approach for estimating soil and vegetation energy fluxes in observations of directional radiometric surface temperature. Agric For Meteorol 77:263–293

Nouri H, Beecham S, Anderson S, Nagler P (2013) High spatial resolution WorldView-2 imagery for mapping NDVI and its relationship to temporal urban landscape evapotranspiration factors. Remote Sens (Basel) 6:580–602. https://doi.org/10.3390/rs6010580

Nouri H, Nagler P, Chavoshi Borujeni S, et al (2020) Effect of spatial resolution of satellite images on estimating the greenness and evapotranspiration of urban green spaces. Hydrol Process 34:3183–3199. https://doi.org/10.1002/hyp.13790

Pahari R, Leclerc MY, Zhang G, et al (2018) Carbon dynamics of a warm season turfgrass using the eddy-covariance technique. Agric Ecosyst Environ 251:11–25. https://doi.org/10.1016/j.agee.2017.09.015

Park G, Park K, Song B, Lee H (2022) Analyzing Impact of Types of UAV-Derived Images on the Object-Based Classification of Land Cover in an Urban Area. Drones 6:. https://doi.org/10.3390/drones6030071

Park S, Ryu D, Fuentes S, et al (2021) Mapping very-high-resolution evapotranspiration from unmanned aerial vehicle (UAV) imagery. ISPRS Int J Geoinf 10:. https://doi.org/10.3390/ijgi10040211

Parker GG (2020) Tamm review: Leaf Area Index (LAI) is both a determinant and a consequence of important processes in vegetation canopies. For Ecol Manage 477

Pastorello G, Trotta C, Canfora E, et al (2020) The FLUXNET2015 dataset and the ONEFlux processing pipeline for eddy covariance data. Sci Data 7:225. https://doi.org/10.1038/s41597-020-0534-3

Qi H, Zhu B, Wu Z, et al (2020) Estimation of peanut leaf area index from unmanned aerial vehicle multispectral images. Sensors (Switzerland) 20:1–15. https://doi.org/10.3390/s20236732

Qin L, Yan C, Yu L, et al (2022) High-resolution spatio-temporal characteristics of urban evapotranspiration measured by unmanned aerial vehicle and infrared remote sensing. Build Environ 222:. https://doi.org/10.1016/j.buildenv.2022.109389

Saher R, Stephen H, Ahmad S (2021) Urban evapotranspiration of green spaces in arid regions through two established approaches: a review of key drivers, advancements, limitations, and potential opportunities. Urban Water J 18:115–127

Saher R, Stephen H, Ahmad S (2022) Role of Urban Landscapes in Changing the Irrigation Water Requirements in Arid Climate. Geosciences (Basel) 13:14. https://doi.org/10.3390/geosciences13010014

Sarkar S, Cazenave AB, Oakes J, et al (2021) Aerial high-throughput phenotyping of peanut leaf area index and lateral growth. Sci Rep 11:. https://doi.org/10.1038/s41598-021-00936-w

Semmens KA, Anderson MC, Kustas WP, et al (2016) Monitoring daily evapotranspiration over two California vineyards using Landsat 8 in a multi-sensor data fusion approach. Remote Sens Environ 185:155–170. https://doi.org/10.1016/j.rse.2015.10.025

Simpson JE, Holman F, Nieto H, et al (2021) High spatial and temporal resolution energy flux mapping of different land covers using an off-the-shelf unmanned aerial system. Remote Sens (Basel) 13:. https://doi.org/10.3390/rs13071286

Simpson JE, Holman FH, Nieto H, et al (2022) UAS-based high resolution mapping of evapotranspiration in a Mediterranean tree-grass ecosystem. Agric For Meteorol 321:. https://doi.org/10.1016/j.agrformet.2022.108981

Stoy PC, Mauder M, Foken T, et al (2013) A data-driven analysis of energy balance closure across FLUXNET research sites: The role of landscape scale heterogeneity. Agric For Meteorol 171–172:137–152. https://doi.org/10.1016/j.agrformet.2012.11.004

Tang Z, Jin Y, Alsina MM, et al (2022) Vine water status mapping with multispectral UAV imagery and machine learning. Irrig Sci 40:715–730. https://doi.org/10.1007/s00271-022-00788-w

Torres-Rua A (2017) Vicarious calibration of sUAS microbolometer temperature imagery for estimation of radiometric land surface temperature. Sensors (Switzerland) 17:. https://doi.org/10.3390/s17071499

Verma B, Prasad R, Srivastava PK, et al (2022) Investigation of optimal vegetation indices for retrieval of leaf chlorophyll and leaf area index using enhanced learning algorithms. Comput Electron Agric 192:. https://doi.org/10.1016/j.compag.2021.106581

Volk JM, Huntington J, Melton FS, et al (2023) Development of a benchmark Eddy flux evapotranspiration dataset for evaluation of satellite-driven evapotranspiration models over the CONUS. Agric For Meteorol 331:109307. https://doi.org/10.1016/j.agrformet.2023.109307

Vulova S, Meier F, Rocha AD, et al (2021) Modeling urban evapotranspiration using remote sensing, flux footprints, and artificial intelligence. Science of the Total Environment 786:. https://doi.org/10.1016/j.scitotenv.2021.147293

Vulova Stenka, Kuhlemann Lena-Marie, Tetzlaff Doerthe, et al (2018) Assessment of evapotranspiration from urban vegetation across space and time: a case study in Berlin. IEEE

Wandera L, Mallick K, Kiely G, et al (2017) Upscaling instantaneous to daily evapotranspiration using modelled daily shortwave radiation for remote sensing applications: An artificial neural network approach. Hydrol Earth Syst Sci 21:197–215. https://doi.org/10.5194/hess-21-197-2017

Wang T, Chandra A, Jung J, Chang A (2022) UAV remote sensing based estimation of green cover during turfgrass establishment. Comput Electron Agric 194:. https://doi.org/10.1016/j.compag.2022.106721

Wang X, Cheng H, Xi J, et al (2018) Relationship between park composition, vegetation characteristics and cool island effect. Sustainability (Switzerland) 10:. https://doi.org/10.3390/su10030587

Wei S, Yin T, Dissegna MA, et al (2020) An assessment study of three indirect methods for estimating leaf area density and leaf area index of individual trees. Agric For Meteorol 292–293:. https://doi.org/10.1016/j.agrformet.2020.108101

Wei Z, Yoshimura K, Wang L, et al (2017) Revisiting the contribution of transpiration to global terrestrial evapotranspiration. Geophys Res Lett 44:2792–2801. https://doi.org/10.1002/2016GL072235

Weiss M, Baret F, Smith GJ, et al (2004) Review of methods for in situ leaf area index (LAI) determination Part II. Estimation of LAI, errors and sampling. Agric For Meteorol 121:37–53. https://doi.org/10.1016/j.agrformet.2003.08.001

Wilber AL, Czarnecki JMP, McCurdy JD (2022) An ArcGIS Pro workflow to extract vegetation indices from aerial imagery of small-plot turfgrass research. Crop Sci 62:503–511. https://doi.org/10.1002/csc2.20669

Wilson K, Goldstein A, Falge E, et al (2002) Energy balance closure at FLUXNET sites

Wu S, Deng L, Guo L, Wu Y (2022) Wheat leaf area index prediction using data fusion based on high-resolution unmanned aerial vehicle imagery. Plant Methods 18:. https://doi.org/10.1186/s13007-022-00899-7

Wutzler T, Lucas-Moffat A, Migliavacca M, et al (2018) Basic and extensible post-processing of eddy covariance flux data with REddyProc. Biogeosciences 15:5015–5030. https://doi.org/10.5194/bg-15-5015-2018

Wynne T, Devitt D (2020) Evapotranspiration of urban landscape trees and turfgrass in an arid environment: Potential tradeoffs in the landscape. HortScience 55:1558–1566. https://doi.org/10.21273/HORTSCI15027-20

Xia T, Kustas WP, Anderson MC, et al (2016) Mapping evapotranspiration with high-resolution aircraft imagery over vineyards using one-and two-source modeling schemes. Hydrol Earth Syst Sci 20:1523–1545. https://doi.org/10.5194/hess-20-1523-2016

Xing Y, Brimblecombe P, Wang S, Zhang H (2019) Tree distribution, morphology and modelled air pollution in urban parks of Hong Kong. J Environ Manage 248:. https://doi.org/10.1016/j.jenvman.2019.109304

Xu T, Liu S, Xu L, et al (2015) Temporal upscaling and reconstruction of thermal remotely sensed instantaneous evapotranspiration. Remote Sens (Basel) 7:3400–3425. https://doi.org/10.3390/rs70303400

Yan G, Hu R, Luo J, et al (2019) Review of indirect optical measurements of leaf area index: Recent advances, challenges, and perspectives. Agric For Meteorol 265:390–411

Zhang J, Virk S, Porter W, et al (2019) Applications of unmanned aerial vehicle based imagery in turfgrass field trials. Front Plant Sci 10:. https://doi.org/10.3389/fpls.2019.00279

Zhu W, Huang Y, Sun Z (2018) Mapping crop leaf area index from multi-spectral imagery onboard an unmanned aerial vehicle. In: 2018 7th International Conference on Agro-Geoinformatics, Agro-Geoinformatics 2018. Institute of Electrical and Electronics Engineers Inc.